Deep-Sea Research I 104 (2015) 72–91

Contents lists available at ScienceDirect

Deep-Sea Research I

journal homepage: www.elsevier.com/locate/dsri

The depth-distribution of nitrogen fixation by *Trichodesmium* spp. colonies in the tropical–subtropical North Atlantic

Elise M. Olson [a,*], Dennis J. McGillicuddy Jr.[a], Sonya T. Dyhrman [b], John B. Waterbury [a], Cabell S. Davis [a], Andrew R. Solow [a]

[a] Woods Hole Oceanographic Institution, MS 9, Woods Hole, MA 02543, USA
[b] Department of Earth and Environmental Science and the Lamont-Doherty Earth Observatory, Columbia University, Palisades, NY 10964, USA

ARTICLE INFO

Article history:
Received 20 August 2014
Received in revised form
26 June 2015
Accepted 29 June 2015
Available online 2 July 2015

Keywords:
Nitrogen fixation
Trichodesmium spp.
North Atlantic
Video Plankton Recorder

ABSTRACT

Nitrogen fixation is an important yet still incompletely constrained component of the marine nitrogen cycle, particularly in the subsurface. A Video Plankton Recorder (VPR) survey in the subtropical North Atlantic found higher than expected *Trichodesmium* colony abundances at depth, leading to the hypothesis that deep nitrogen fixation in the North Atlantic may have been previously underestimated. Here, *Trichodesmium* colony abundances and modeled nitrogen fixation from VPR transects completed on two cruises in the tropical and subtropical North Atlantic in fall 2010 and spring 2011 were used to evaluate that hypothesis. A bio-optical model was developed based on carbon-normalized nitrogen fixation rates measured on those cruises. Estimates of colony abundance and nitrogen fixation were similar in magnitude and vertical and geographical distribution to conventional estimates in a recently compiled climatology. Thus, in the mean, VPR-based estimates of volume-specific nitrogen fixation rates at depth in the tropical North Atlantic were not inconsistent with estimates derived from conventional sampling methods. Based on this analysis, if *Trichodesmium* nitrogen fixation by colonies is underestimated, it is unlikely that it is due to underestimation of deep abundances by conventional sampling methods.

1. Introduction

The balance (or imbalance) of the marine nitrogen cycle has been subject to much debate (Codispoti et al., 2001; Deutsch et al., 2007; Galloway et al., 2004; Gruber, 2004, 2008). During the 1980s, questions arose from apparent disparities between new production estimates based on oxygen utilization rates and those based on the combination of net primary production measured by ^{14}C incubation with estimated recycling efficiencies within the euphotic zone (e.g. Jenkins and Goldman, 1985; Platt and Harrison, 1985; Shulenberger and Reid, 1981). Assessments of the summed sources and sinks of fixed nitrogen to the global oceans have produced varying results due to differing estimates of water column and benthic denitrification rates (Gruber, 2008). Results range from near balance (Gruber, 2004, 2008) to modest (Galloway et al., 2004) or large, 200 Tg N yr^{-1} (Codispoti et al., 2001), imbalance. The imbalance may be comparable to total global nitrogen fixation, which has been estimated between 100 and 150 Tg N yr^{-1} (Gruber, 2008). True imbalance might be associated with anthropogenic perturbation (Codispoti et al., 2001; Galloway et al., 2004; Gruber, 2008); however, Deutsch et al. (2007) argue for balance on the basis of tight coupling between nitrogen fixation and denitrification. Other means of resolving the apparent imbalance are downward revision of denitrification estimates or upward revision of estimates of sources, such as nitrogen fixation.

A study by Davis and McGillicuddy (2006) presented the possibility that the imbalance might result from underestimation of nitrogen fixation by *Trichodesmium*. Their Video Plankton Recorder (VPR) survey captured greater than expected *Trichodesmium* colony abundance at depth in the northern limb of the North Atlantic subtropical gyre. This apparent discrepancy with prior studies could be due to the VPR's noninvasive sampling technique. In contrast, net tows and Niskin bottles may disrupt fragile colonies, particularly when they are sampled at depth and must travel farther to reach the surface. Davis and McGillicuddy (2006) posited that if similarly-shaped abundance profiles were present in the regions where *Trichodesmium* is most abundant, such as the

Abbreviation: VPR, Video Plankton Recorder; PAR, photosynthetically active radiation; ADT, absolute dynamic topography

* Corresponding author.
E-mail addresses: eolson@whoi.edu (E.M. Olson), dmcgillicuddy@whoi.edu (D.J. McGillicuddy Jr.), sdyhrman@ldeo.columbia.edu (S.T. Dyhrman), jwaterbury@whoi.edu (J.B. Waterbury), cdavis@whoi.edu (C.S. Davis), asolow@whoi.edu (A.R. Solow).

http://dx.doi.org/10.1016/j.dsr.2015.06.012
0967-0637/

southwestern North Atlantic, deep *Trichodesmium* populations could potentially account for the "missing" nitrogen.

Here, we have evaluated that hypothesis, using data collected by VPR during fall 2010 and spring 2011. We examined mesoscale and larger variability in the depth distribution of colonies and its association with physical processes. A bio-optical nitrogen fixation model, developed from nitrogen fixation assays carried out during the two cruises, was used to infer nitrogen fixation rates from VPR abundance data.

2. Materials and methods: data collection

Sampling occurred on the R/V *Oceanus* from October 1–22, 2010 (OC469) to April 23–May 13, 2011 (OC471), beginning near Bermuda and ending near Barbados (Fig. 1). Precise sampling locations were informed by satellite observations of sea surface height, real-time analysis of VPR *Trichodesmium* abundance observations, and ocean-color-based estimates of *Trichodesmium* bloom probability (Westberry and Siegel, 2006; Westberry et al., 2005). This adaptive strategy allowed sampling to be directed toward interesting physical and biological features such as eddies and areas of potentially elevated *Trichodesmium* abundance. Regions of both low and high abundance were sampled. A series of cyclonic and anticyclonic eddies were transected during each cruise.

2.1. Nitrogen fixation rate measurements

The sampling program included daily stations with associated nitrogen fixation experiments (Heithoff, 2011) beginning at approximately 10:00 a.m. local time in order to capture the period of

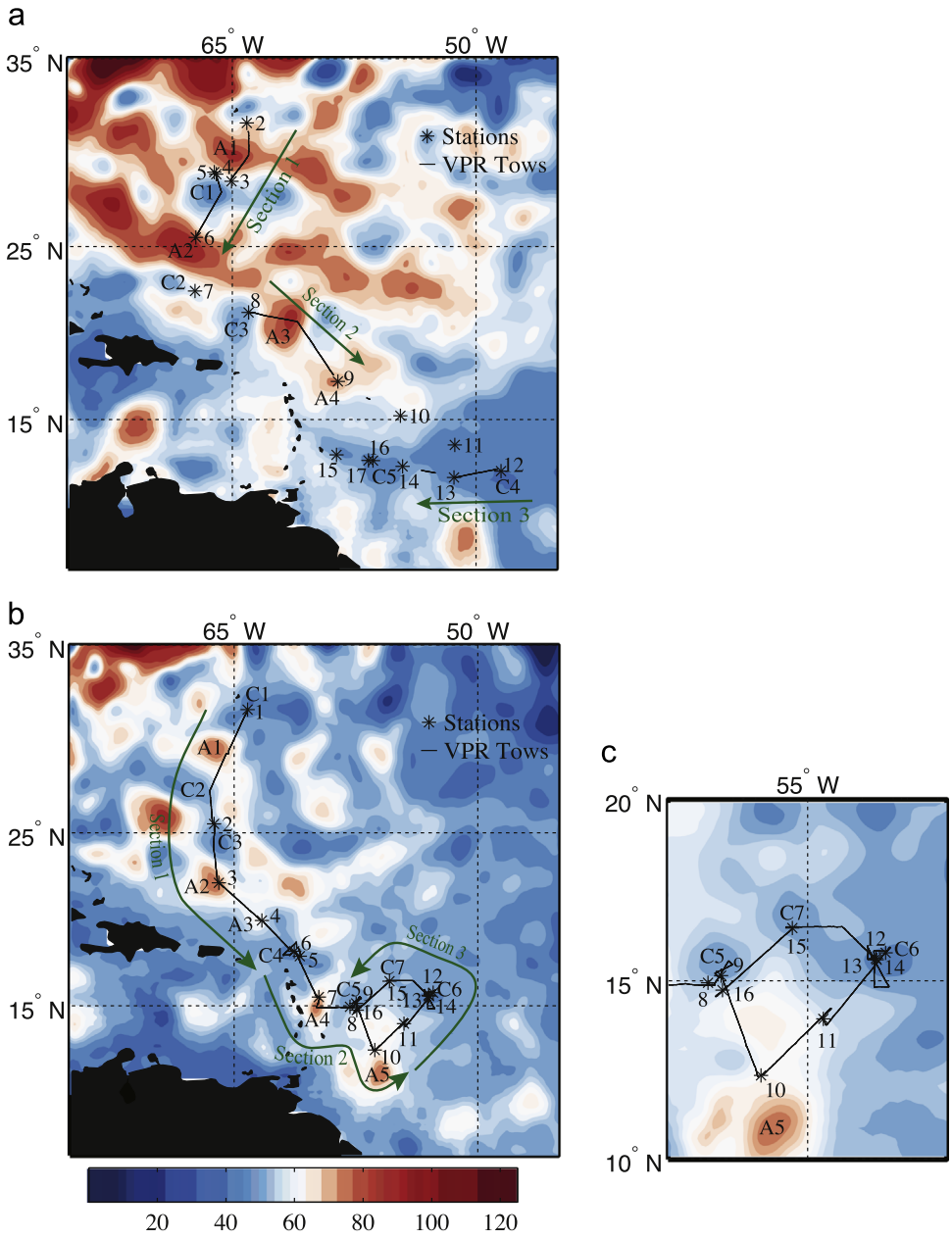

Fig. 1. Locations of stations and VPR tows for (a) the fall cruise and (b) the spring cruise with absolute dynamic topography (ADT) in cm. Black lines indicate VPR tows. Stars indicate station locations. Targeted cyclonic and anticyclonic eddies are labeled with prefixes "C" and "A", respectively. Labeled sections (arrows) are referred to in subsequent analysis. ADT was calculated by objective analysis of available altimetry data from Envisat and Jason-1/2. (c) Southwestern portion of the spring cruise track and altimetry magnified and for a later date (May 8, 2011), when cyclone C7 was more apparent.

peak diurnal nitrogen fixation. *Trichodesmium* colonies for onboard incubation experiments were picked individually with pipettes from water collected near the surface (5–15 m) and at depth (20–70 m). Surface and deep samples were collected by pumping water into a 130 μm mesh net on the fall cruise and by MOCNESS with 150 μm mesh nets on the spring cruise. Additional near-surface samples were taken by manual 1/3 m hand net tows (130 μm mesh) between the surface and approximately 10 m depth on both cruises. After initial collection, individual colonies were isolated using eyedroppers and transferred to 0.2 μm local filtered seawater for incubation experiments in order to assemble sufficient biomass to produce measurable rates.

Nitrogen fixation was measured by acetylene reduction assay using the theoretical 3:1 conversion ratio for ethylene production to dinitrogen fixation (Capone and Montoya, 2001), after Rodier and Borgne (2010), Hutchins et al. (2007), and Mulholland et al. (2006). A recent study by Wilson et al. (2012a) using a modified and improved $^{15}N_2$ method found that the ratio of C_2H_4 production to $^{15}N_2$ assimilation varied from 7 to 27 on surface seawater samples from the North Pacific. However, we have continued with the conventional ratio in order to facilitate comparisons with previous measurements.

In brief, roughly 20 colonies were assayed in 60 mL polycarbonate bottles with 30 mL of headspace, with time points measured at regular intervals over an incubation period of roughly 3 h. Incubations in the shipboard Percival incubator (Percival Scientific) were carried out at temperatures of 26.0–27.5 °C. Irradiances generally corresponded to *in situ* PAR within the limitations of the incubators. The maximum irradiances attainable were 400 μmol quanta m^{-2} s^{-1} during the fall cruise and 700 μmol quanta m^{-2} s^{-1} during the spring cruise. Additional deck-board nitrogen fixation experiments were carried out during the spring cruise at natural irradiances ranging from 1000 to 1600 μmol quanta m^{-2} s^{-1}.

For each nitrogen fixation sample, the numbers of puff and raft colonies were recorded. Colonies were filtered onto a combusted GF/F filter using vacuum filtration, and CHN analysis was performed by the Marine Biological Laboratory Stable Isotope Laboratory in Woods Hole, MA. These data were used to estimate carbon per puff and raft colony for each cruise by linear regression.

2.2. Hydrography and discrete water sampling

At each station, temperature, salinity, and PAR were measured through CTD casts. Water samples were collected with a rosette system in 10 L Niskin bottles at depths of 80, 60, 40, 20 m, and the surface for phosphate analyses and the microscopic enumeration of *Trichodesmium* colonies and free trichomes by methods described by Carpenter et al. (2004). In brief, samples were gravity filtered onto 10 μm, 47 mm diameter filters through in-line filter holders attached to the spigots of the Niskin bottles. The filters were fixed for 30 min in the filter holders with 4% paraformaldehyde in 0.2 μm filtered sea water. Paraformaldehyde was removed and the filters were then mounted in immersion oil on slides with coverslips. The fixed preparations were stored frozen prior to enumeration. *Trichodesmium* spp. colonies and filaments (trichomes) were identified and counted with epifluorescence microscopy of phycoerythrin autofluorescence by imaging the entire filter. Colonies were defined as associations of 8 or more filaments. Colonies and filaments were enumerated in 70 samples from 14 stations from the fall cruise. From the spring cruise, colonies were enumerated in 43 samples from 9 stations, and filaments were enumerated in 39 samples from the same 9 stations. Water for nutrient analyses was filtered through a 0.2 μm PC filter into acid-cleaned bottles and stored frozen. Low level phosphate concentrations were measured in the upper 100 m using a modified MAGIC method (Rimmelin and Moutin, 2005) with a detection limit of 2.5 nM.

2.3. Video Plankton Recorder sampling

Trichodesmium colony abundance was sampled by the VPR, towed between stations (Fig. 1). The VPR provided a noninvasive sampling method and high spatial resolution, facilitating observation of phenomena occurring at the mesoscale and even submesoscale. It consists of a towed body, containing a CTD, fluorometer, PAR (photosynthetically active radiation) and oxygen sensors, and a synchronized video camera and xenon strobe (Davis et al., 2005). The VPR undulated between the surface (5–10 m) and approximately 120 m depth, completing an up-down cycle approximately every six minutes, or every 1.8 km at 10 knots. At a frame rate of 30 Hz, each 984 × 1009 pixel (roughly 13 × 13 mm) video frame was passed through object-identification software to pick out "regions of interest" and save them, using a time-stamp naming convention, to a hard disk.

Images were initially sorted using image recognition software (Hu and Davis, 2006). For the spring cruise, due to the large number of images collected, the sample size was reduced to 1000 images per sampling hour, evenly spaced among the collected images (Olson, 2014). For both cruises, each machine image classification was manually checked and reclassified as necessary, into the three *Trichodesmium* morphological categories (puff, raft, and bowtie) and an "other" category containing everything else. We classified fusiform or roughly parallel arrangements of trichomes as rafts, round colonies as puffs, and colonies with splayed edges and constricted middles as bowties. *Trichodesmium* puff, raft, and bowtie colonies were readily sampled using the VPR system due to their macroscopic size, but individual trichomes were not distinguishable from other similarly shaped bodies. Although the three morphotypes constitute a useful practical basis for image classification, genetic studies have demonstrated a lack of correspondence between morphological characteristics of colonies and clade or species differentiation (Hynes et al., 2012; Orcutt et al., 2002; Rouco et al., 2014).

Data from the fall cruise were gridded to 11 km wide by 5 m deep bins. Data from the spring cruise were gridded to wider 33 km by 5 m bins to compensate for the reduction in sample density due to subsampling. Within each bin, abundances were estimated based on the number of positive identifications per category and the volume sampled, with spring cruise sample volumes adjusted to equal the fraction of images classified multiplied by the original sample volume. The volume of the field of view was calibrated before each cruise by the tethered copepod method described by Davis et al. (2005), and was 6.929 mL and 15.168 mL during the fall and spring cruises, respectively.

Microscopic colony counts made at stations were compared to the nearest available VPR colony abundances to confirm the calibration of the VPR sampling volume and the image subsampling method applied to data from the spring cruise (Olson, 2014) (Appendix A, Fig. A1). Microscopic colony counts demonstrated significant correlation with VPR colony abundances ($R=0.94$, $p < 0.001$, $n=43$ for spring and $R=0.61$, $p=0.016$, $n=15$ for fall) despite the spatial and temporal separation of paired samples and patchiness of *Trichodesmium* distributions.

Physical and bio-optical data from the VPR were binned to the same horizontal resolution as the abundance data and either 1 or 5 m vertically, as indicated. Mixed layer depths were diagnosed using a threshold criterion of 0.125 kg m^{-3} difference in potential density from the surface, based on binned data at 1 m vertical resolution. Since the VPR does not sample the uppermost 5–10 m of the water column, some surface stratification was missed. However, the threshold criterion used typically successfully

identified the depth of a pycnocline characterized by elevated buoyancy frequency. The mixed layer depth, as diagnosed by the 0.125 kg m^{-3} difference from the uppermost CTD measurement, was within the upper 5 m in only three out of 31 stations on the two cruises, and within the upper 10 m for seven, six of them in a low salinity lens.

3. Calculations: data analysis and modeling

A bio-optical model was developed and applied to VPR transects. The results were compared with a previous model used by Davis and McGillicuddy (2006) and with a climatology (Luo et al., 2012). The development and implementation of the model, the implementation of the Davis and McGillicuddy (2006) model for comparison purposes, and an assessment of sources of error in the model are detailed in the following sections.

3.1. Bio-optical model

We estimated daily volume-specific nitrogen fixation rates over the VPR transects by combining VPR colony abundance estimates, PAR estimates, and a bio-optical model for nitrogen fixation (summarized in Fig. 2). Although temperature dependence of *Trichodesmium* nitrogen fixation has been demonstrated in the literature, the effect was not included because data collected in the present study were not sufficient to constrain such a relationship (Appendix B).

Several studies have developed functional relationships between nitrogen fixation and irradiance based on a saturating response of nitrogen fixation to PAR, with or without photoinhibition (Hood et al., 2002; Breitbarth et al., 2008; Davis and McGillicuddy, 2006). The relationships are based on data from nitrogen fixation assays on samples collected at sea and in culture and are characterized by constant slope at low irradiance with asymptotic approach to maximum nitrogen fixation (in the absence of photoinhibition). In the present study, the high light incubation experiments did not provide convincing evidence of photoinhibition of nitrogen fixation. Thus, we related carbon-normalized nitrogen fixation rates to irradiance using a hyperbolic tangent function:

$$F = \mu \tanh(\alpha I/\mu) \quad (1)$$

where F is the carbon-normalized nitrogen fixation rate, I is the irradiance, α is the initial slope of the F–I curve, and μ is the maximum carbon-normalized nitrogen fixation rate in the limit of saturating I. The parameters associated with the relationship (μ and α, Eq. (1)) were fit by maximum likelihood estimation to nitrogen fixation and incubation irradiance from acetylene reduction assays on field-collected samples from the fall and spring cruises (Fig. 3) under an assumption of normally distributed random error.

Despite slightly lower nitrogen fixation rates during the fall cruise, fitting the model to the combined data from both cruises reduced the parameter uncertainty as diagnosed by the breadth of the 95% confidence intervals (Fig. 3). The lower nitrogen fixation rates during the fall cruise may reflect true variability or result from methodological differences. Incubation light levels used during the fall cruise were lower, and disruption of colonies by the pump sampling method is a possibility. The pump method resulted in smaller volumes sampled and less biomass collected, perhaps giving rise to decreased likelihood of encountering healthy, active colonies. However, carbon-normalized nitrogen fixation rates did not scale with carbon biomass per sample except for a few of the smallest samples. Material collected from hand net tows at the same stations came from a broader range of depths but had nitrogen fixation rates similar to or higher than surface pump samples.

The estimation of daily nitrogen fixation rates based on the nitrogen fixation–incubation irradiance relationship is complicated by diel variation of nitrogen fixation rates. The approach taken was to input instantaneous irradiance modeled at twelve minute intervals (Appendix C) directly into Eq. (1) and integrate

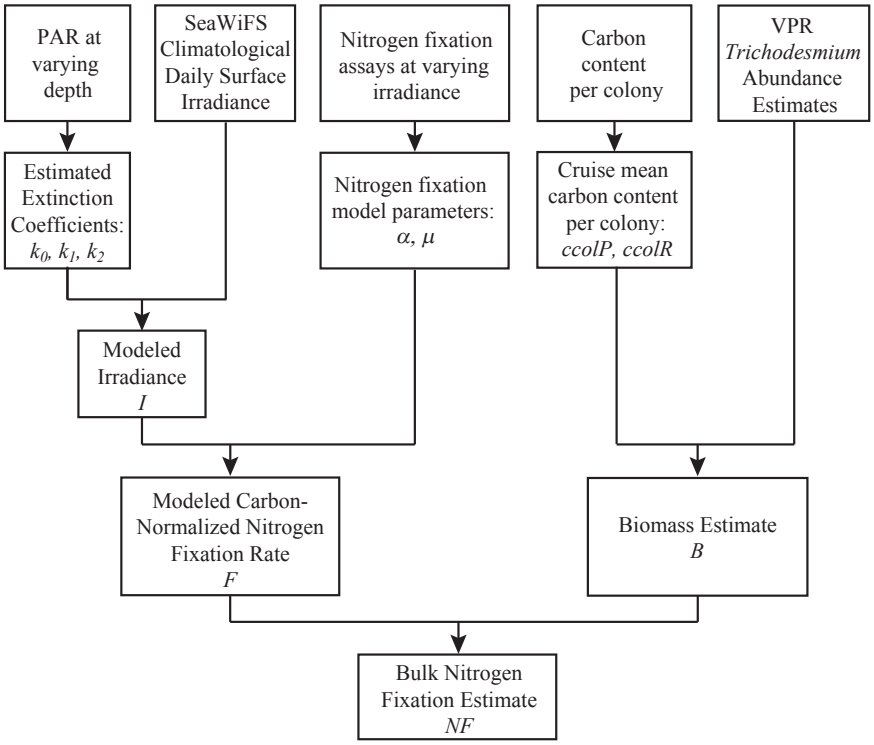

Fig. 2. Diagram of flow of information used to model daily volume-specific nitrogen fixation (nitrogen fixation per liter of water per day).

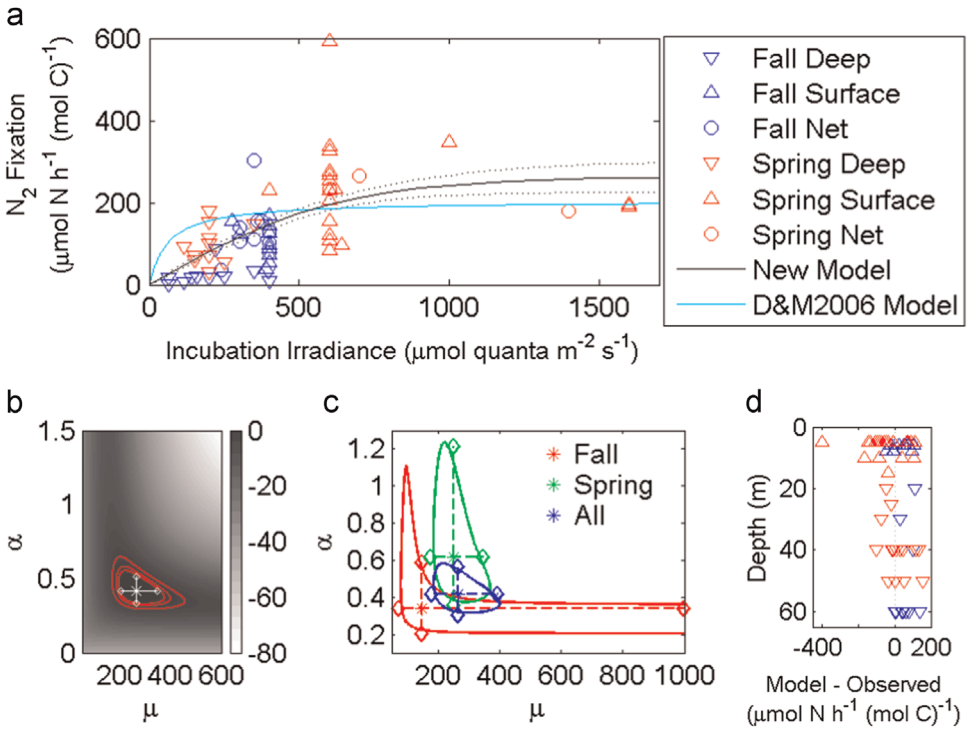

Fig. 3. (a) Nitrogen fixation as a function of incubation irradiance. Symbols differentiate cruises and colony sources. Surface and deep samples were collected from discrete depths by pump in fall and MOCNESS in spring, while hand net samples collected on both cruises integrated over the upper water column (see Section 2.1). A solid black line represents the least squares fit to Eq. (1), based on all available data from the fall and spring cruises. Dashed lines indicate model upper and lower bounds based on estimated standard error. (b) Profile log likelihood of observations based on model Eq. (1) and normally distributed error. Asterisk indicates maximum likelihood estimate for all parameters (σ, α, and μ), while red contours indicate 90, 95, and 99% confidence regions. White lines demarcate profile log likelihood 95% confidence intervals for each parameter individually, with the others at maximum likelihood estimates. (c) 95% confidence regions when parameters are assessed based on data from the fall cruise (red), data from the spring cruise (green) and both cruises combined (blue). (d) Residuals in the fit relating nitrogen fixation to light, as a function of depth. Also shown in (a) adapted version of the Davis and McGillicuddy (2006) model (cyan). In order to present the adapted Davis and McGillicuddy (2006) model in these axes, we converted from per-colony to per-carbon nitrogen fixation by dividing by the overall mean (puffs and rafts from both cruises) carbon to colony ratio of 6.182e−7 mol C (colony)$^{-1}$ and assumed a midday surface light intensity of 1600 μmol quanta m^{-2} s^{-1}.

over a day. Although the nitrogen fixation–irradiance relationship is based on measurements made at the time of day nitrogen fixation is generally observed to be maximum, the procedure results in a diel pattern that is qualitatively consistent with the canonical pattern of *Trichodesmium* nitrogen fixation: increase from morning to midday, decrease from midday to sunset, and absence just before or shortly after dark. This type of diel pattern was present in several previous studies (Fu and Bell, 2003; Chen et al., 1996; Ohki et al., 1992; Saino and Hattori, 1978). Data from the present study were not sufficient to constrain a more complex mechanistic representation of diel variability.

The light model incorporated surface irradiance based on SeaWiFS climatological PAR in order to represent average conditions. Irradiance at depth was estimated from surface values using extinction coefficients derived from VPR PAR observations made during each cruise (Appendix C). Prior to input to the model, irradiance was averaged within the mixed layer under the simplifying assumption that colonies were continuously randomly redistributed within the layer. Mixed layer depth is an indication of the past history of mixing in a given location, and does not necessarily indicate current active mixing to a given depth. However, it was the best indicator of the depth of mixing based on the available data.

Daily carbon-normalized nitrogen fixation rates were multiplied by carbon biomass to estimate total daily rates (Fig. 2). Biomass was estimated by multiplying a morphology- and cruise-specific mean carbon content per colony (Appendix D) by the number of colonies per volume at each grid location of the binned abundance data described above. Model standard error was estimated using a second order Taylor expansion (Appendix E).

3.2. *Application of Davis and McGillicuddy (2006) model*

For comparison, we also present rates calculated with the model used by Davis and McGillicuddy (2006). They framed their model in terms of per-colony nitrogen fixation, with a surface rate of 0.7 nmol N(mol C)$^{-1}$ h^{-1} based on nitrogen-fixation incubations on diver-collected colonies reported by Orcutt et al. (2001). In that study, rates from diver-collected colonies were approximately four times higher than corresponding rates measured on net-sampled colonies. In order to carry out a more balanced comparison between the Davis and McGillicuddy (2006) model and the present model, we scaled the surface nitrogen fixation rate in the Davis and McGillicuddy (2006) model to match the overall mean per-colony surface (≤10 m) nitrogen fixation rate from the present study of 0.13 nmol N(mol C)$^{-1}$ h^{-1} (multiplying the Davis and McGillicuddy, 2006 model by a factor of 0.13/0.7). We also modified the conversion from hourly to daily rates to adjust for the three-hour nitrogen fixation incubations of the present study. This correction consisted of multiplication of the Davis and McGillicuddy (2006) model by a factor of 0.6533/0.7353, equal to the inverse of the ratio of the mean value a half sinusoid over the present three-hour incubation period to the mean value over the seven-hour period described by Davis and McGillicuddy (2006). In this conversion, we retained the Davis and McGillicuddy (2006) assumption of sinusoidal modulation of nitrogen fixation between zero and a maximum rate over the course of a twelve-hour light period.

In addition to applying the Davis and McGillicuddy (2006) model to VPR abundance data from the present study, we applied our new model to the abundance profiles published by Davis and McGillicuddy (2006). The following values were assumed: surface irradiance of 38 mol quanta m^{-2} d^{-1} based on mission composite SeaWiFS PAR for the region, a vertical extinction coefficient of 0.05 m^{-1}, a mixed layer depth of 30 m, and mean carbon per colony for puffs and rafts estimated from fall 2010 data, which was collected at nearly the same time of year as the Davis and McGillicuddy (2006) survey, but in a different region.

3.3. Model assessment

Detailed examination of the nitrogen-fixation–irradiance fit revealed some systematic errors (Fig. 3). Nitrogen fixation was higher in spring than fall, so the fit tended to overestimate fall values and underestimate spring values. Additionally, surface-collected samples tended to have higher rates than deep samples at similar incubation light levels, particularly for the fall cruise, a tendency not reproduced by the model. There was a slight tendency for the model to underestimate surface nitrogen fixation and overestimate deep nitrogen fixation, particularly for the fall cruise.

In order to evaluate uncertainty in the nitrogen fixation estimates, a side-by-side comparison from a sample transect (Fig. 4) of modeled *Trichodesmium* nitrogen fixation was made with model standard error based on propagation of variance in each of the parameters (Appendix E). In most locations, the standard error was less than one-quarter of the estimated value.

Modeled nitrogen fixation rates were compared with rates estimated directly from incubation experiments under an assumption of sinusoidal modulation of nitrogen fixation throughout the light period (Fig. 5). Exact correspondence was not expected due to the different conversion from hourly to daily rates, basis of the modeled values on climatological irradiance, and variability not reproduced by the model. Nonetheless, there was strong correspondence between modeled nitrogen fixation rates and rates estimated directly (correlation coefficient = 0.98, $p < 0.01$; linear regression: $y = 1.07x + 0.19$). Rates calculated based on the Davis and McGillicuddy (2006) model (based on percent of surface irradiance rather than absolute PAR) more strongly deviated from

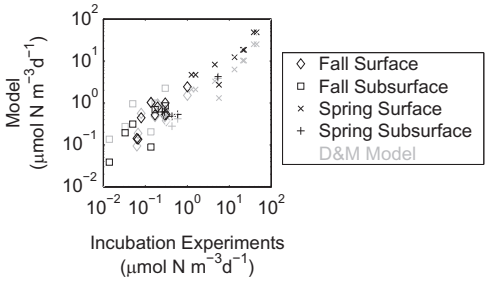

Fig. 5. Comparison between modeled *Trichodesmium* nitrogen fixation rates (using the model presented here and the Davis and McGillicuddy, 2006 model) and rates estimated from incubations under the assumption of sinusoidal modulation of nitrogen fixation throughout the daylight period.

the observed nitrogen fixation rate compared to the model fit to the current nitrogen fixation rates (standard error of 8.1 μmol N m^{-3} d^{-1} compared to 3.6 μmol N m^{-3} d^{-1}).

Our simple approach to the modeling of nitrogen fixation as a function of light omits several factors that have been shown to influence the modulation of nitrogen fixation. For instance, studies have demonstrated latent effects of previous light exposure (Heithoff, 2011; Wilson et al., 2012b). The nitrogen fixing capacity represented in our model may in reality adjust gradually to changes in light conditions. Additionally, the response to light may vary across species and ecotypes. At low light levels, spectral variation has been demonstrated to influence *Trichodesmium* nitrogen fixation rates in addition to intensity (Fu and Bell, 2003; Wilson et al., 2012b). Diel variation in nitrogen fixation by *Trichodesmium* has been linked to a variety of complex cellular-level processes such as circadian rhythm (Chen et al., 1996), nitrogenase synthesis, energy availability, and response to cellular carbon and nitrogen reserves (Rabouille et al., 2006). Despite these caveats, our approach produces a daily nitrogen fixation curve qualitatively consistent with several previous studies (Fu and Bell, 2003; Chen et al., 1996; Ohki et al., 1992; Saino and Hattori, 1978) and nearly equivalent in daily integral to the sinusoidal modulation assumed by Davis and McGillicuddy (2006) (see Fig. 5).

Nitrogen fixation rates are also influenced by factors other than light. Iron and phosphorus availability can affect the physiological state of the colonies and their nitrogen fixation rates (Sanudo-

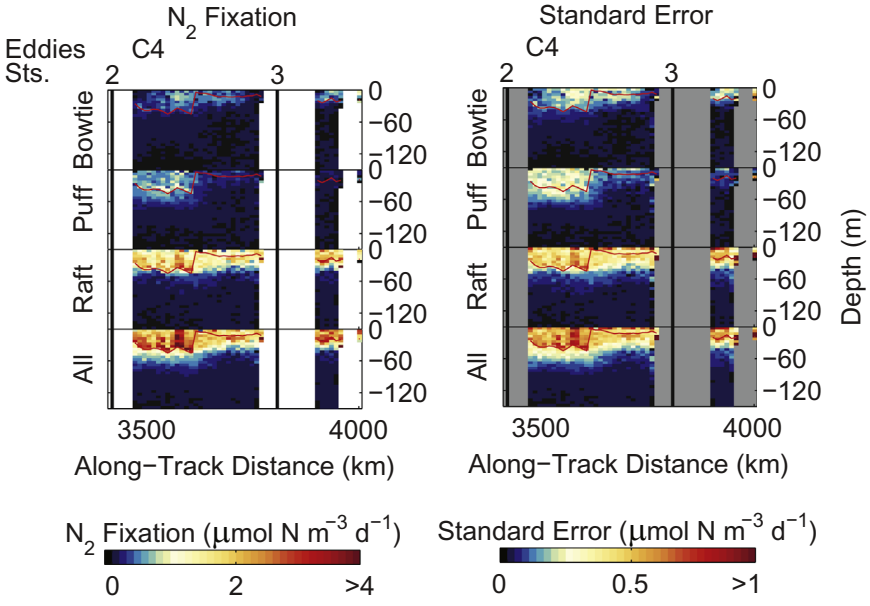

Fig. 4. Nitrogen fixation estimates for fall cruise VPR Section 3 (left) and associated approximate model standard error (right). Color scales differ by a factor of four.

Wilhelmy et al., 2001; Orchard et al., 2009; Berman-Frank et al., 2007; Mills et al., 2004). In fact, Heithoff (2011) found a statistically significant anticorrelation between nitrogen fixation rate and *Trichodesmium* alkaline phosphatase activity during the fall cruise, suggesting an impact of phosphorus stress on nitrogen fixation. These drivers could affect bulk nitrogen fixation rates both through impacts on carbon-normalized nitrogen fixation and through influence on biomass. The latter were represented to an extent through the directly estimated colony abundance, but the former were not. Carbon content per colony was estimated using mean values, and therefore any covariation between colony size and per-carbon nitrogen fixation rate could be a source of model error. Thus, variable iron and phosphorus availability and other factors influencing physiological status could cause actual nitrogen fixation patterns to differ from those simulated.

Another source of uncertainty was nitrogen fixation by free filaments. Whereas nitrogen fixation assays were carried out only on the more readily sampled colonial morphologies, free filaments were also present everywhere *Trichodesmium* was abundant. Free filament biomass was calculated at stations where microscope filament counts were available. We assumed a ratio of 3.091 nmol carbon per filament, based on the average carbon per colony from the two cruises of 0.6182 μmol and an assumed filament content of 200 per colony, as in Luo et al. (2012). The carbon content of free filaments was assumed the same as that of colonial filaments. Free filaments made up approximately 6.7% of *Trichodesmium* biomass on the fall cruise and 9.8% on the spring cruise, or 8.2% overall based on pooled data from both cruises (Fig. 6). The fraction was reasonably consistent across cruises and abundance levels, and was similar to previously reported levels in the region. For example, Carpenter et al. (2004) reported cruise free filament fractions ranging from 7 to 11% in the tropical North Atlantic. To estimate total nitrogen fixation including fixation by filaments, one might multiply the rates presented below by 1.09 (the mean ratio of free to colonial filaments, corresponding to a free filament biomass fraction of 8.2%, is 0.09). However, as rates of nitrogen fixation by free filaments were not measured, such a correction was not made.

The model was designed to capture that portion of the depth-variability of *Trichodesmium* nitrogen fixation that can be attributed to a relationship with light. It cannot reproduce local variability due to other drivers. We therefore apply the model to the estimation of regional mean nitrogen fixation profiles rather than attempting to resolve fine-scale horizontal patterns.

4. Results and discussion

We present and discuss VPR-observed patterns in the depth distribution of *Trichodesmium* colony abundance. In Section 4.1, we consider associations between these patterns and their physical setting as well as implications for nitrogen fixation rates based on the bio-optical model. In Section 4.2, we compare regional mean depth profiles based on the present study with previous findings.

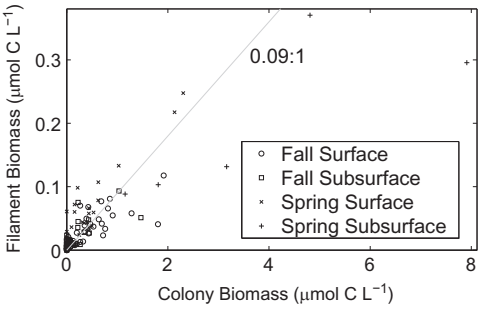

Fig. 6. Filament to colony biomass ratio.

4.1. Mesoscale to sub-basin-scale patterns in the depth-distribution of *Trichodesmium* colony abundance: associations with physical properties and implications for nitrogen fixation

The VPR data provided the opportunity to assess mesoscale variations in colony distribution by morphology. Genetic analysis of samples collected on these cruises revealed that while the overall abundance of *Trichodesmium* colonies correlated with the distribution of the two dominant *Trichodesmium* clades (I and III), individual clade distributions did not relate well to colony morphology (Rouco et al., 2014). This suggests that colony morphology is not necessarily a strong indicator of *Trichodesmium* species in this dataset. Nonetheless, variations in depth distribution of colonies by morphology may be indicative of niche differentiation (Post et al., 2002).

The canonical view of strongly surface-intensified *Trichodesmium* colony abundance was broadly upheld in the present study in the southwestern North Atlantic. In the mean, colony abundance peaked in the near-surface and decreased with depth. It was highest within the mixed layer throughout most of the region sampled. This tendency was most pronounced in raft abundances from Section 1 and Eddy C4 (Fig. 7a) from the fall cruise and Section 1 from the spring cruise as well as abundances of all colony morphologies in Eddies A4 and A5 from the spring cruise (Fig. 7b). The coincidence of vertical gradients in biomass, particularly of rafts, with gradients in density suggests that stratification may act as a barrier to the mixing of buoyant colonies deeper in the water column.

The various *Trichodesmium* colony morphologies were distributed differently with depth over much of the region sampled. Rafts, typically the most abundant morphology, generally exhibited the most strongly skewed distribution with depth. The tendency for greater abundance within the mixed layer is consistent with greater floating velocities observed in raft colonies (Walsby, 1978). In contrast, in some areas, puff biomass was uniformly distributed with depth throughout the upper 150 m, consistent with conditions observed over parts of the transatlantic VPR survey by Davis and McGillicuddy (2006). This was typical of the lower abundance northern portion of the region sampled in the present study (e.g. Section 1, spring and fall). Similar distributions of the colony morphologies have been observed in other studies, with more rafts typically located higher in the water column (Post et al., 2002).

An exception to this pattern was observed over part of the southernmost region sampled on the spring cruise (Fig. 7b, Section 3 and part of Section 2), where all morphologies were similarly distributed with depth and abundances were nearly equal. Anomalously fresh water was encountered there, likely of riverine origin, mixed to around 60 m depth in Eddy A4 but confined elsewhere to a shallow surface lens. Throughout much of this region, except for Eddies A4 and A5, there was not a large gradient in colony abundance at the base of the mixed layer.

The southern, fresh-water influenced region sampled during the spring cruise included the highest integrated colony abundances observed on either of the two cruises, with local maxima in anticyclonic Eddies A4 and A5 (Fig. 7b). A similar trend with salinity was present in the distribution of clades over a smaller sample set from the spring cruise (Rouco et al., 2014). Amazon River freshwater input has been suggested as an explanation for elevated phytoplankton abundance tied to nitrogen fixation in the southwestern North Atlantic by Coles et al. (2004). Subramaniam et al. (2008) and Tovar-Sanchez and Sañudo-Wilhelmy (2011) also described support of diazotrophy through outflow from the

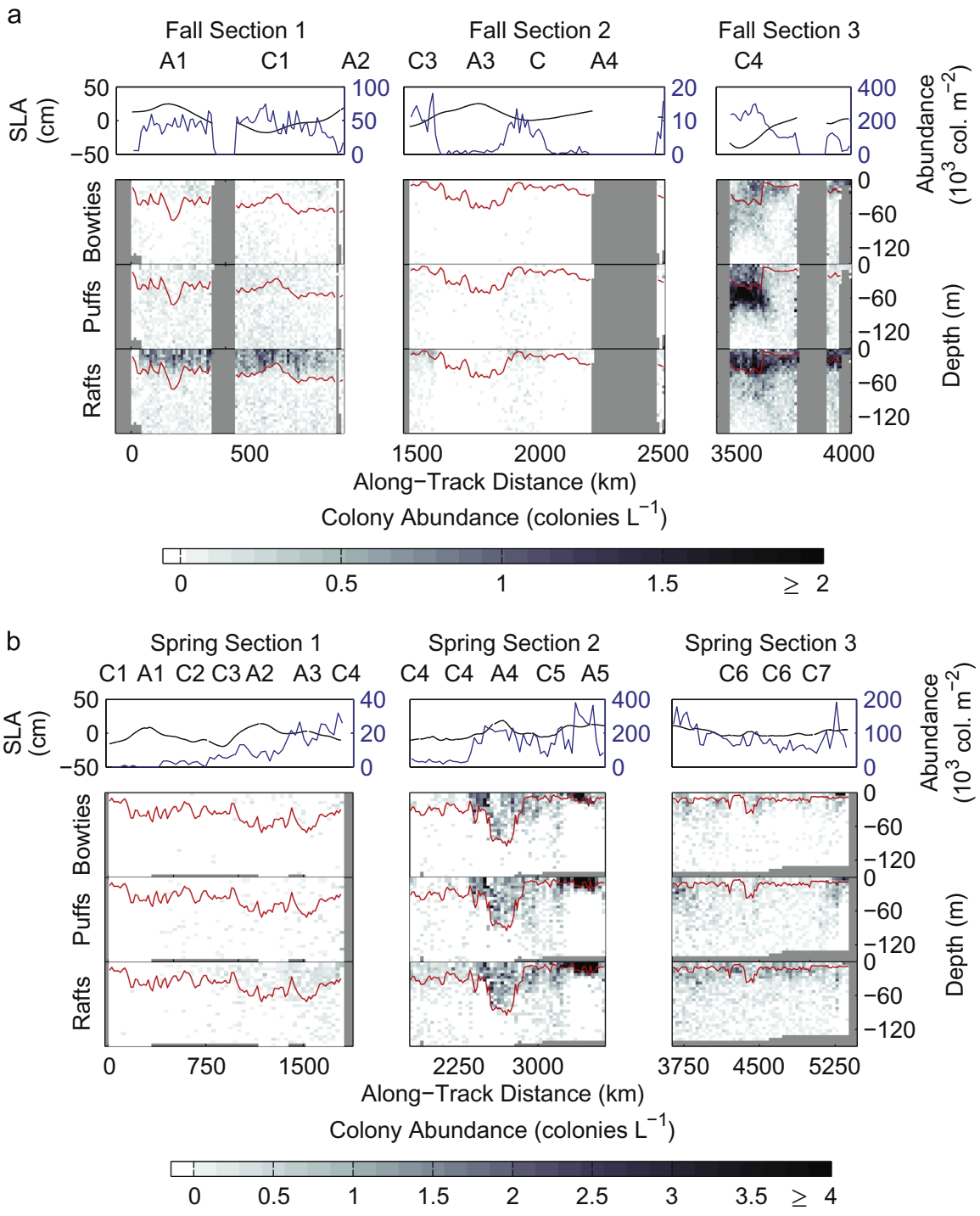

Fig. 7. (a) Fall and (b) spring *Trichodesmium* colony abundance from VPR observations. For each set, the top panel displays sea level anomaly (black) and depth-integrated abundance (blue). The lower three panels show abundance by colony morphology. Red lines designate mixed layer depth. Gray areas are regions not sampled by VPR. Eddies are identified by the prefix "C" for cyclones or "A" for anticyclones and a number indicating the sequence in which the cyclones and anticyclones were encountered on each cruise.

Amazon and Orinoco rivers transporting nutrients far into the tropical Atlantic. Thus, the co-occurrence of elevated *Trichodesmium* biomass with anomalously fresh water may have been related to nutrient input through river outflow. Additionally, stratification is thought to be conducive to *Trichodesmium* growth by confining the colonies to the well-illuminated strata of the near-surface region.

The highest integrated colony abundances were encountered in a thin lens in anticyclonic Eddy A5. There, colony abundance was more strongly surface-intensified than anywhere else on the cruise (Fig. 8e). This distribution could be explained by both the strong stratification due to the presence of a freshwater lens and the rapid extinction of light in the turbid riverine surface water, possibly due to dissolved organic matter of riverine origin or biological material originating from nutrients supplied through the river plume. The highest phosphate in near-surface waters (0.15 μM compared to a mean of 0.03 μM at 40 m) was observed below the mixed layer at Station 10, near the center of Eddy A5. If *Trichodesmium* colonies were able to migrate vertically there (e.g. Letelier and Karl, 1998; Villareal and Carpenter, 2003; White et al.,

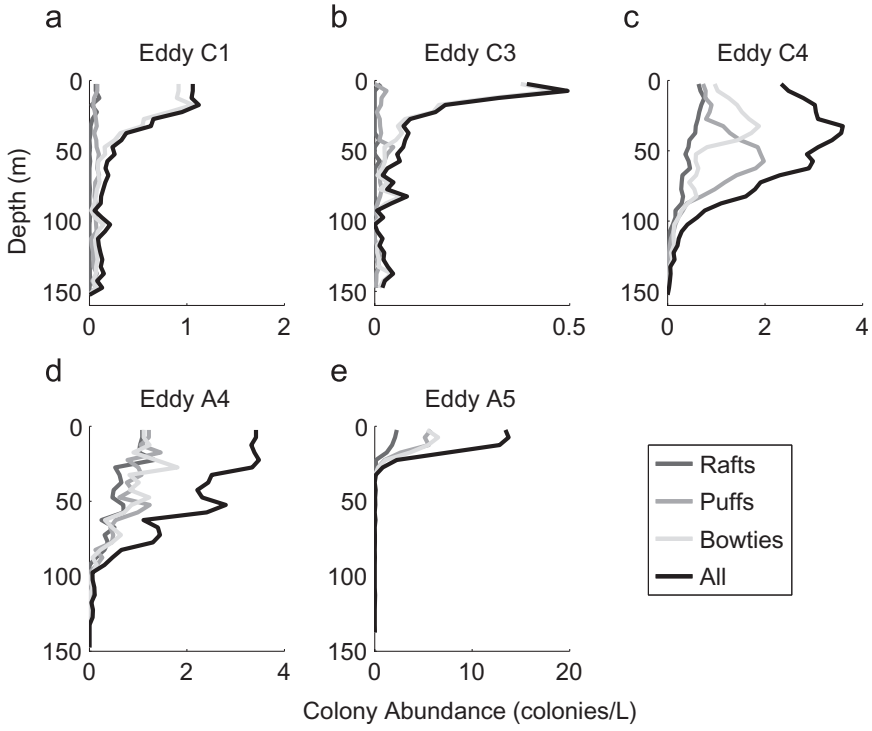

Fig. 8. Abundance versus depth by colony morphology for regions with varied physical characteristics from the two cruises: (a) fall cruise Eddy C1; (b) fall cruise Eddy C3; (c) fall cruise Eddy C4; (d) spring cruise Eddy A4; and (e) spring cruise Eddy A5 (with freshwater lens). Upper three panels are from the fall cruise and lower two panels are from the spring cruise.

2006), access to this phosphate could promote their growth; however, very few colonies were observed below the surface layer and stratification was strong. Of the various types of abundance profiles described in White et al. (2006), the observations at Station 10 appear to be most consistent with surface trapping, rather than one of the distributions associated with vertical migration.

Although typical profiles of colony abundance featured peaks at or near the surface and rapid decay with depth, there were two locations in which colony abundances were unusually elevated at depths of approximately 40–80 m. These were spring cruise Eddy A4 and fall cruise Eddy C4 (Fig. 7). Together, the two sites comprised approximately 700 km (roughly 10%) of the total track length sampled by the VPR. Both were characterized by local deepening of the mixed layer.

Spring cruise Eddy A4, described earlier, featured deeply mixed low salinity water, elevated colony abundances, and roughly consistent depth-distributions of each of the three morphologies (Fig. 8d). Colony abundances of all morphologies peaked near the surface but decreased more gradually with depth than was typical.

In contrast, the elevated colony abundance at depth in fall cruise Eddy C4 was due to a subsurface peak in puff abundance. The peak just below the mixed layer in Eddy C4 (Fig. 7a, Section 3; Fig. 8c) was the densest concentration of puffs observed throughout the fall cruise. However, as in the transatlantic section (Davis and McGillicuddy, 2006), this local maximum in puff colony abundance was small compared to peaks in raft abundances observed elsewhere. Due to the influence of the puff distribution in Eddy C4, maxima in mean puff and raft abundance over the cruise as a whole were vertically distinct. The mixed layer in Eddy C4 was deeper than the surroundings.

Perhaps the puffs in fall cruise Eddy C4 were the remnants of a bloom that initiated closer to the surface and subsequently sank. Alternatively, the profile is consistent with distributions produced through simulation of phosphorus mining behavior (Type 3, White et al., 2006). No phosphate measurements were taken within the feature. However, at nearby stations, phosphate concentrations became measurable by the low-level method at depths of 80 m (0.04 μM). Yet another possibility is that the colonies were adapted to thrive at these depths. The location of the peak below the mixed layer in low light conditions may indicate that puffs filled a different niche from the surface-dwelling rafts, as suggested by Post et al. (2002) on observation of a subsurface maximum. Thus, it is possible that this atypical feature in the puff distribution may also have unique physiological characteristics reflecting low light adaptation. Physiological adaptations to low irradiance have been observed in *Trichodesmium* in culture, including increased cell diameter for light absorption and changes in coupling of phycobilisomes with the photochemical reaction centers (Andresen et al., 2010). Consistent with this possibility, Rouco et al. (2014) found depth segregation of clades in data from the spring cruise only where the mixed layer was anomalously deep, as it was in fall cruise Eddy C4.

Physiological adaptations could be accompanied by differences in nitrogen fixation rates. No nitrogen fixation samples were taken from within the subsurface puff maximum, so it is impossible to test this particular prediction. The potential of this type of subsurface puff feature to fix nitrogen at depth warrants further investigation through direct rate measurements, and the VPR is an ideal tool to identify potential sampling sites. Extending over a distance of only approximately 100 km along the cruise track, the feature could easily have been missed by more discrete sampling methods. Although the feature was unique within the present study, puff colony abundances peaked at depth in other studies in locations such as the western subtropical Atlantic (Davis and McGillicuddy, 2006) and the Gulf of Aqaba in the Red Sea (Post et al., 2002).

The model described in Section 3 suggests that colonies located close to the surface contribute more to nitrogen fixation than those at depth due to the attenuation of light. Additionally, the lower carbon content of puffs compared to rafts over the cruise as

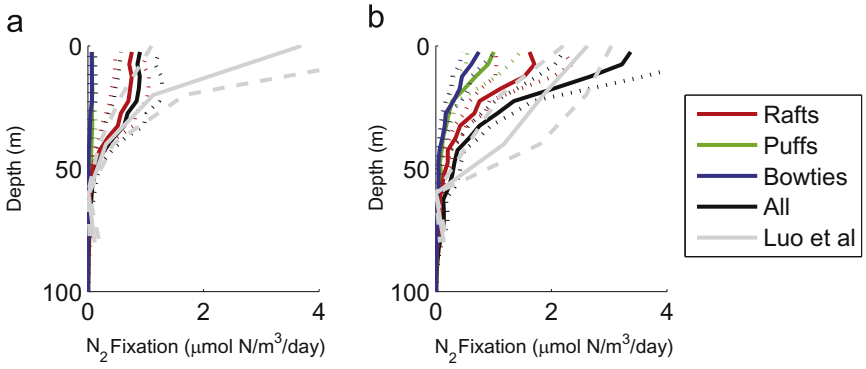

Fig. 9. Mean profiles of modeled nitrogen fixation versus depth for the (a) fall and (b) spring cruises. Dashed lines represent the standard error of the mean. Gray line is mean of depth-binned values from Luo et al. (2012) dataset for similar location (within 500 km) and season (within 90 year-days) to VPR track, with gray dotted lines representing standard error of the mean.

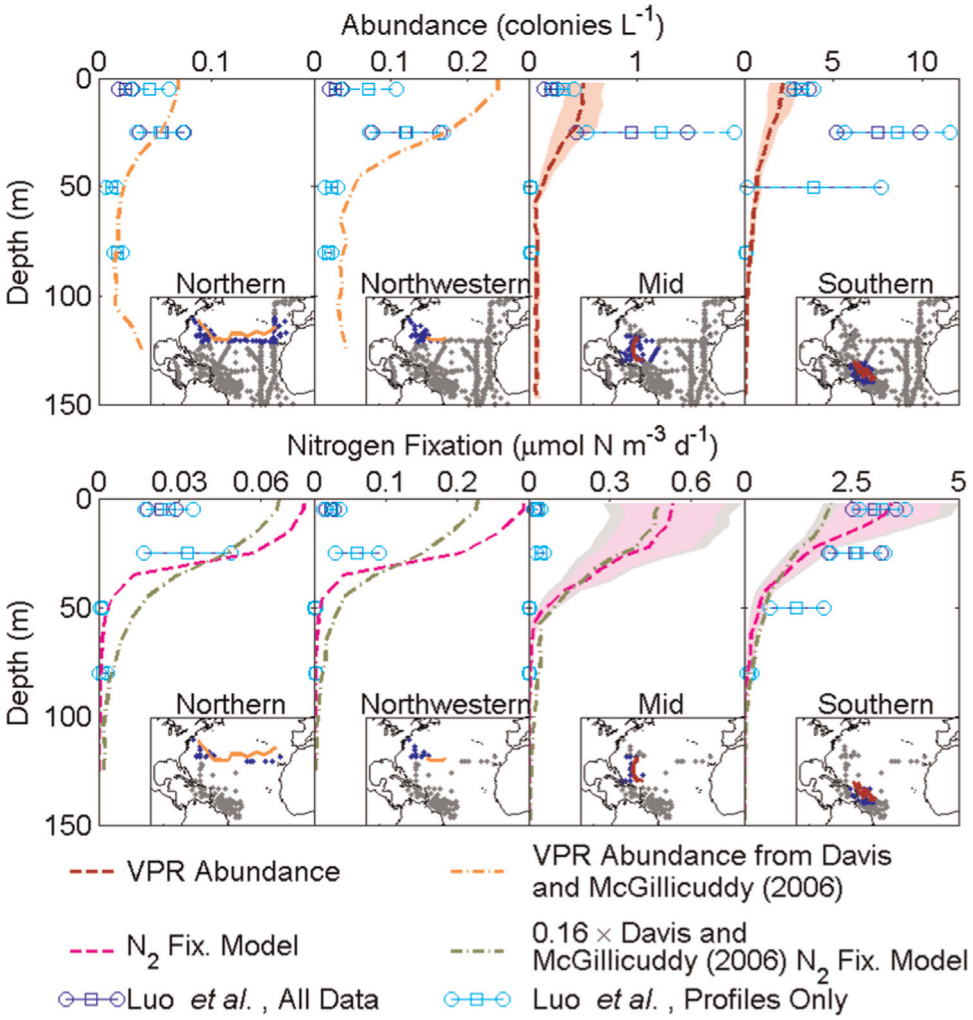

Fig. 10. Mean depth profiles of *Trichodesmium* abundance (upper) and *Trichodesmium* nitrogen fixation (lower) for several regions in the North Atlantic. The profiles were based on mean data from Luo et al. (2012) (squares) with standard error of the mean (circles) and VPR-based estimates (dashed lines). Estimates in dark blue were based on all Luo et al. (2012) data in each bin while only stations with measurements at two or more depths were included in the profile calculations (cyan). The geographical distribution of data from the Luo et al. (2012) database for each region is shown on an inset map in blue, over the total distribution of data points from Luo et al. (2012) in gray. VPR transects are overlaid on the maps in orange (transects from Davis and McGillicuddy, 2006) and red (transects from the present study). From left to right, the regions are northern (75–8°W, 28–40°N); northwestern (75–50°W, 29–40°N); mid (75–50°W, 20–32°N); and southern (65–50°W, 10–20°N). Also shown are nitrogen fixation rates estimated from the VPR abundances and the nitrogen fixation model developed here (magenta) as well as the adapted (multiplied by a factor of 0.16) version of the nonlinear model presented in Davis and McGillicuddy (2006) (green). The models were applied to the Davis and McGillicuddy (2006) mean abundance profiles (northern and northwestern), whereas for the regions sampled in the present study (mid and southern) they were applied at all locations before taking the means. VPR abundance and modeled nitrogen fixation profiles from the present study are surrounded by light red and magenta shaded regions representing the standard error of the mean. The outer gray region surrounding the nitrogen fixation mean profiles represents additional uncertainty based on the standard error associated with the model (Table 1, rightmost column).

a whole suggests a reduced contribution of this puff maximum to local *Trichodesmium* carbon. However, the model was based on rate measurements dominated by colonies of the more abundant raft morphology. Therefore, any difference in the light-dependence of nitrogen fixation between puffs and rafts is not reflected in the predicted rates for the deep population of puffs in fall Eddy C4.

Overall, the present findings provide little support for the hypothesis that deep populations of *Trichodesmium* colonies are present and fixing significant quantities of nitrogen in the southwestern North Atlantic. Application of the nitrogen-fixation–light model to the VPR-based colony abundance transects suggests only modest levels of nitrogen fixation at depths greater than 40 m, consistent with previous findings (Fig. 9). In order to reconcile these results with the findings of Davis and McGillicuddy (2006), we next compare both studies to previously collected data compiled by Luo et al. (2012).

4.2. *Large-scale spatial variations in nitrogen fixation: comparisons with Luo et al. (2012) and Davis and McGillicuddy (2006)*

VPR-based *Trichodesmium* colony abundance and modeled nitrogen fixation rates from the present study and based on Davis and McGillicuddy (2006) (applied as described in Section 3.2) were compared with data extracted from the set of conventionally sampled observations compiled by Luo et al. (2012) in corresponding geographic domains (Fig. 10). The conventional methods used to collect the data included in the Luo et al. (2012) database were light microscopy on samples collected by net or Niskin bottle for abundances, and acetylene reduction or $^{15}N_2$ assimilation experiments for nitrogen fixation. We report mean profiles of colony abundance and nitrogen fixation along with error bounds based on the standard error of the mean and the standard error associated with the model where applicable (see Appendix E). We interpret the sum of these two types of error as an indicator of the uncertainty associated with estimated mean modeled nitrogen fixation profiles.

Differences between the VPR data and the Luo et al. (2012) climatology were not surprising considering the different geographical and temporal coverage of the datasets. The most significant was that, except in the southernmost region, conventional mean surface abundances were lower than VPR estimates. Subsurface maxima were present in the conventional mean vertical abundance profiles for all four regions analyzed (Fig. 10; northern, northwestern, mid, and southern) but not the regional mean VPR-based abundance profiles. The subsurface maximum in the Luo et al. (2012) data appeared even when calculations were restricted to stations with measurements at two or more depths ("profiles only" in Fig. 10).

This inconsistency might have been attributable to a difference in vertical location of the surface sample, since the VPR normally approached no closer than within 5 m of the surface, whereas net or bottle samples may have been taken in the upper one to two meters. Based on microscopic enumeration of colonies from bottle samples, 10 out of 15 stations from the fall cruise and 1 out of 8 from the spring cruise had lower abundances in the surface bottle sample than in one of the deeper samples from the same station. Thus, the difference in surface VPR-based abundances may simply reflect temporal variability.

Based on the conventionally-derived profiles, the lower abundances in the northern region were more uniform with depth than the southern profiles, consistent with VPR observations by Davis and McGillicuddy (2006). However, even in the northern region, greatest variability and average abundance occurred in the upper 40 m. Both the VPR-based estimates and the newly available compilation of traditionally sampled data (Luo et al., 2012) demonstrated greater abundance and nitrogen fixation rates compared to the conventional profiles used in Davis and McGillicuddy (2006) to compare with their VPR data. Through analysis of the more extensive Luo et al. (2012) data we saw that the relatively high abundance and inferred nitrogen fixation at depth described by Davis and McGillicuddy (2006) were characteristic of the subtropical North Atlantic region that they sampled, but not of the higher abundance region to the south.

Mean nitrogen fixation based on Luo et al. (2012) was elevated in the 20–40 m range relative to the surface in the northern, northwestern and mid regions, but these subsurface peaks were less pronounced than in the abundance data (Fig. 10). Bio-optical VPR nitrogen fixation estimates were higher than the conventionally sampled estimates, particularly at the surface, in the three northernmost regions. Modeled and conventional nitrogen fixation profiles agreed most closely in the southern region, with the error bars overlapping in the top and bottom bins, and near adjacency in the middle two bins. As in abundance, there was a southward increase in both amplitude and vertical extent of nitrogen fixation in both the conventionally sampled and bio-optically modeled profiles. Mean rates in the 40–60 m range from the southern profile were nearly 40% of surface levels and were higher than mean surface rates in the northern profile. Deeper rates, at 60–100 m depth, were approximately an order of magnitude lower than in the 40–60 m range, contributing only a small fraction of depth-integrated nitrogen fixation. In the southern region, agreement between the models and observations in the Luo et al. (2012) database was strongest.

The present bio-optical model of nitrogen fixation estimated higher rates near the surface and lower rates at depth compared to the adapted Davis and McGillicuddy (2006) model, despite a tendency for the present model to overestimate deep nitrogen fixation rates. The difference between the models could be explained by comparing their nitrogen-fixation–light responses under mean midday conditions (Fig. 3). The Davis and McGillicuddy (2006) model approached its asymptotic nitrogen fixation value at lower light levels. Surface irradiance did not impact the Davis and McGillicuddy (2006) model, in which nitrogen fixation was a function of the fraction of irradiance relative to the surface.

Depth-integrated abundances and nitrogen fixation rates from the fall and spring cruises fell within the range of conventionally-derived estimates, although the more spatially and temporally diverse data from Luo et al. (2012) exhibited greater variability and higher peak values (not shown). Given the degree of variability among nearby measurements in the Luo et al. (2012) dataset, we attribute the differences between the Luo et al. (2012) mean values and the present study to temporal variability. Broad geographical patterns were similar, with nitrogen fixation increasing from the subtropics to the tropics in both spring and fall. Just as Davis and McGillicuddy (2006) observed higher abundances in the western portion of their VPR transect, profiles based on data west of 50°W in the 29–40°N range of the Luo et al. (2012) data were elevated compared to data from the full extent of the North Atlantic at those latitudes. Across the regions analyzed (Fig. 10), abundances increased progressively to the south, with the mid region elevated compared to the northwestern region and the southern region higher still.

Application of the model for nitrogen fixation presented in this study to the Davis and McGillicuddy (2006) colony abundance profile for the wider northern region (Fig. 10 bottom left panel and Table 1) yielded an integrated nitrogen fixation rate of 2.3 μmol N m^{-2} d^{-1}, much lower than the 16.74 μmol N m^{-2} d^{-1} estimated by Davis and McGillicuddy (2006). However, modification of their estimate by the factor of 0.16 for consistency of surface nitrogen fixation rates with those measured in the present study reduced the Davis and McGillicuddy (2006) estimate to

Table 1
Vertically integrated nitrogen fixation estimates (μmol N m^{-2} d^{-1}) for the regions presented in Fig. 10. The standard error of the mean is estimated at each depth within each profile and the delta method is applied (Appendix E). For the new model, the standard error associated with the model itself (Model SE) is also reported (gray regions in Fig. 10, lower right panels). The standard error is not available for the two mean profiles (northern and northwestern) originating from the Davis and McGillicuddy (2006) study.

Region	Luo et al. (2012)-based		Adjusted Davis and McGillicuddy (2006) model		New model		
	NF	SE	NF	SE	NF	SE	Model SE
Northern	1.2	0.40	2.7		2.3		
Northwestern	1.9	0.70	8.1		8.2		
Mid	1.6	0.39	19	2.0	18	2.1	0.67
Southern	145	24	76	6.7	94	11	3.3

2.7 μmol N m^{-2} d^{-1}, nearly identical to the OC469–OC471 new model estimate. The integrated nitrogen fixation based on profiles available in Luo et al. (2012) was slightly lower at 1.2 μmol N m^{-2} d^{-1}. The difference of a factor of about 6 between the daily surface nitrogen fixation rates (based on diver-collected samples) used by Davis and McGillicuddy (2006) and those estimated in the present study was roughly consistent with the factor of 4 difference in nitrogen fixation reported by Orcutt et al. (2001) between diver- and net-collected samples, with some of the additional difference likely due to spatial and temporal variability.

Additional methodological biases could contribute to variability in nitrogen fixation estimates. Both acetylene reduction and $^{15}N_2$ assimilation methods can be biased due to incomplete gas equilibration (Wilson et al., 2012b). Mohr et al. (2010) reported that nitrogen fixation may be underestimated by the $^{15}N_2$ incubation method due to failure of injected $^{15}N_2$ gas bubbles to reach equilibrium with the water. The degree of underestimation depends on the incubation duration as the $^{15}N_2$ bubble equilibrates with the water over time. Whereas the current study includes only nitrogen fixation measurements based on acetylene reduction assays, the Luo et al. (2012) database also included nitrogen fixation measurements from $^{15}N_2$ incubations. However, Luo et al. (2012) reported that nitrogen fixation rates from both methods distributed over a similar range. This apparent consistency between methods was verified for each of the four regions in which mean profiles were examined (Appendix F). Additional uncertainty in nitrogen fixation estimates made by acetylene reduction assay stemmed from the choice of conversion ratio between acetylene reduction and nitrogen fixation. A ratio of 3 was used in the present study, whereas Luo et al. (2012) report ratios of 3 or 4.

Modifying the Davis and McGillicuddy (2006) estimate for nitrogen fixation in the northwest subtropical Atlantic of 50.54 μmol N m^{-2} d^{-1} by the factor of 0.16 produces an estimate of 8.1 μmol N m^{-2} d^{-1}, nearly the same as the OC469–OC471 new model estimate of 8.2 μmol N m^{-2} d^{-1}. In that region, the estimate based on Luo et al. (2012) was 1.9 μmol N m^{-2} d^{-1}. There, as well as in the mid region, modeled nitrogen fixation estimates based on the VPR were high compared to mean profiles from the Luo et al. (2012) data. Since the abundance estimates in these regions were consistent with Luo et al. (2012), considering the level of variability in the data, it seemed likely that this discrepancy was due to spatial and temporal variability in per-carbon nitrogen fixation rates.

Integrated nitrogen fixation for the southern region (Fig. 10 bottom right panel) based on the VPR survey mean profile was estimated at 94 μmol N m^{-2} d^{-1}, or 76 μmol N m^{-2} d^{-1} using the adjusted Davis and McGillicuddy (2006) model. The integrated nitrogen fixation rate based on the mean profiles from the Luo et al. (2012) data in this region was 145 μmol N m^{-2} d^{-1}. All of these estimates fell in the lower end of the range of areal nitrogen fixation rates reported by Capone et al. (2005) in the southwestern tropical North Atlantic, reflecting the relatively low rates measured on these cruises.

5. Conclusions

The high-resolution sampling made possible by the VPR revealed covariation of *Trichodesmium* colony distributions with characteristics of the physical environment. Colony abundances were typically elevated within the mixed layer, suggesting that physical mixing is of primary importance in determining the depth-distribution. In some regions, vertical distributions differed by colony morphology, with rafts centered higher in the water column than puffs. Deep colony populations were encountered in localized regions making up approximately 10% of the track sampled.

These observations of infrequent instances of elevated deep colony abundance are consistent with previous findings. The new data therefore do not provide evidence that conventional sampling methods have underestimated deep *Trichodesmium* colony populations due to disruption of deep colonies. However, this study could not prove absence of depth-bias in conventional sampling relative to VPR sampling of *Trichodesmium* colonies because the two methods were not applied to the same samples. Nonetheless, means and large-scale spatial trends in VPR-observed *Trichodesmium* colony distributions were consistent with prior observations from the Luo et al. (2012) database. This consistency promotes confidence in the efficacy of the newer imaging-based VPR method.

In the mean, estimated nitrogen fixation rates at depth that are not appreciably larger than previous measurements in the Luo et al. (2012) database. Although the present model tends to overestimate nitrogen fixation at depth, this error does not weaken that conclusion. However, in addition to limitations of the model, the measurements themselves have associated uncertainty. Both $^{15}N_2$ incubation and acetylene reduction nitrogen fixation assays are susceptible to systematic underestimation (Mohr et al., 2010; Wilson et al., 2012a). Additionally, the present model was calibrated with rates from pump- and net-collected samples, which Davis and McGillicuddy (2006) suggested could be low due to mechanical disturbance of the colonies during sampling, based on comparisons of rates from net- and diver-collected samples by Orcutt et al. (2001). This could explain why the present study did not predict deep nitrogen fixation levels in the tropical North Atlantic as high as hypothesized by Davis and McGillicuddy (2006) based on rates from diver-collected samples. Deficiencies in standard techniques for the measurement of nitrogen fixation rates may contribute more significantly to underestimation of nitrogen fixation than uncertainties in abundance.

Compared to the northern region sampled by Davis and McGillicuddy (2006), nitrogen fixation profiles from the tropical Atlantic exhibited higher rates. In mean profiles encompassing all VPR sections from the present study, 28% of colonies were below 50 m depth, but these colonies contribute only 7% of total bio-optically estimated nitrogen fixation. Mean nitrogen fixation and abundance profiles were not inconsistent with mean profiles calculated from the Luo et al. (2012) dataset based on the confidence intervals. However, the Luo et al. (2012) mean profiles revealed abundance and nitrogen fixation levels comparable to those at the surface as deep as 50 m. The pattern of nearly uniform *Trichodesmium* puff colony abundance with depth throughout the upper 120 m described by Davis and McGillicuddy (2006) may be more typical of low-abundance regions sampled in that study.

The VPR observations from the present study demonstrated high abundance deep *Trichodesmium* populations only in specific and infrequent circumstances, consistently associated with anomalously deep mixed layers. Comparison with Luo et al. (2012) data showed that both the Davis and McGillicuddy (2006) colony abundance profiles and those from the present study were typical of their respective regions, confirming that the observed differences in vertical distribution were attributable to regional differences. Colony morphology may be a significant factor in determining the vertical distribution of nitrogen fixation, as depth distributions varied in some regions by morphology. A striking example was the cluster of puff colonies below the mixed layer observed during the fall cruise. Unresolved variability in nitrogen fixation rate by morphology or ecotype could lead to error in deep nitrogen fixation estimates. Future studies could include nitrogen fixation experiments on puff colonies collected from a similar deep cluster. Perhaps genetic studies of the *Trichodesmium* clade distribution in the vicinity of the puff aggregation could shed some light on its origin and physiology. Further study could leverage a combination of VPR observation and net tows to specifically target patches of deep colonies and measure their nitrogen fixation rates.

Acknowledgments

We sincerely thank the officers and crew of the R/V *Oceanus* as well as the science participants. A. Heithoff conducted the nitrogen fixation assays at sea. M. Oates assisted with VPR image classification. H. Joy-Warren completed the microscopic enumeration of colonies. G. Flierl provided valuable feedback on this work. Toby Westberry provided ocean-color-based estimates of *Trichodesmium* bloom probability during the two cruises. Satellite PAR data from the SeaWiFS sensor were processed by the Ocean Biology Processing Group at NASA's Goddard Space Flight Center (http://oceancolor.gsfc.nasa.gov). Altimeter products were produced and distributed by AVISO (www.aviso.oceanobs.com/) as part of the SSALTO ground processing segment. V. Kosnyrev assisted in the analysis of altimetric data. We gratefully acknowledge support of this research by NSF and NASA. A NASA Earth and Space Science Fellowship supported E. Olson's graduate studies.

Appendix A. Comparison of abundance estimates from VPR and microscopy

Samples used for microscopic enumeration at stations were paired with binned means of the nearest available VPR abundance data. Exact correspondence was not expected due to the spatial separation of the sample locations for microscopic enumeration and locations of VPR sampling. A low bias in VPR-based estimates was evident above approximately 1.5 colonies L^{-1}, abundance levels which were only encountered in station–VPR data pairs from the spring cruise.

Appendix B. Assessment of temperature as a potential nitrogen fixation model parameter

Previous studies have indicated that the effects of temperature may be primary drivers of *Trichodesmium* nitrogen fixation rates on a global scale (Breitbarth et al., 2007; Levitan et al., 2010). *Trichodesmium* nitrogen fixation has a narrow optimal temperature range, peaking at approximately 27 °C in IMS-101 (an isolate of *T. erythraeum*) based on culture experiments (Breitbarth et al., 2007). Chappell and Webb (2010) reported optimal temperatures

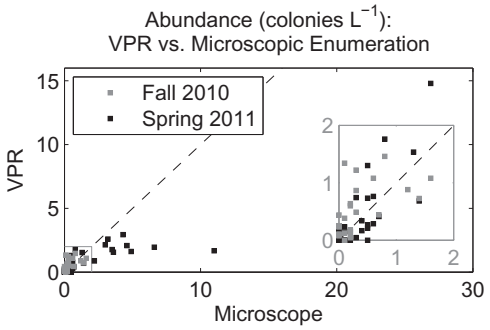

Fig. A1. Comparison between estimates of *Trichodesmium* colony abundance based on the VPR and microscopic enumeration for nearest available measurements. Inset shows enlargement of the lower right corner of the plot, showing abundances less than 2 colonies L^{-1}. The results of a linear regression of VPR onto microscopic abundances were $y = 0.48x + 0.20$ for all data; $y = 0.71x + 0.18$ for abundances less than 2 colonies L^{-1}.

for growth of 28 °C for the *T. erythraeum* clade and 26 °C for the *T. tenue* clade (including *T. thiebautii*), suggesting that temperature may be a factor contributing to niche differentiation between clades.

A correlation between carbon-specific nitrogen fixation rate and temperature could not be assessed based on the present data because all incubations were carried out within a limited temperature range from 26.0 to 27.5 °C. Application of the Breitbarth et al. (2007) nitrogen-fixation–temperature relationship to VPR temperature sections (Fig. B1) showed that with few exceptions, *Trichodesmium* was most abundant within its optimal temperature range for nitrogen fixation. Based on Breitbarth's temperature–nitrogen-fixation curve, the reduction of nitrogen fixation rate from its maximum value due to temperature would be less than 20% for 86% of colonies observed during the fall cruise and 99% of colonies during the spring cruise (Fig. B1c). The temperature effect would be less than 10% for 86% of colonies from the spring cruise. Based on this limited effect and the absence of data from the present study with which to test the relationship, we decided not to include temperature dependence of nitrogen fixation in the present model. Nonetheless, temperature dependence may have played a role in shaping the distribution of colonies, based on the location of the majority of *Trichodesmium* colonies in areas with favorable temperatures and the observation of greater *Trichodesmium* colony abundances during the spring cruise when waters were warmer.

Appendix C. PAR model

In situ PAR input to the nitrogen fixation model (see Fig. 2) was itself modeled by extrapolating SeaWiFS 8-day climatological daily surface PAR to depths using attenuation coefficients estimated from VPR PAR data. Climatological SeaWiFS observations have the advantages of broader spatial and temporal coverage than the available VPR PAR measurements. The SeaWiFS climatological values represent PAR just below the sea surface under average conditions, including the effects of cloud-cover. Eight-day periods close to the middle of each cruise were selected from available SeaWiFS climatologies: October 8–15 (1997–2010) for the fall cruise and May 1–8 (1998–2010) for the spring cruise.

It is common to determine a vertical attenuation coefficient that is approximately constant in time for a given water composition, regardless of time of day (Kirk, 1994). We adopted this idealized approach, modeling PAR at depth based on surface PAR and vertical attenuation coefficients, k, defined as

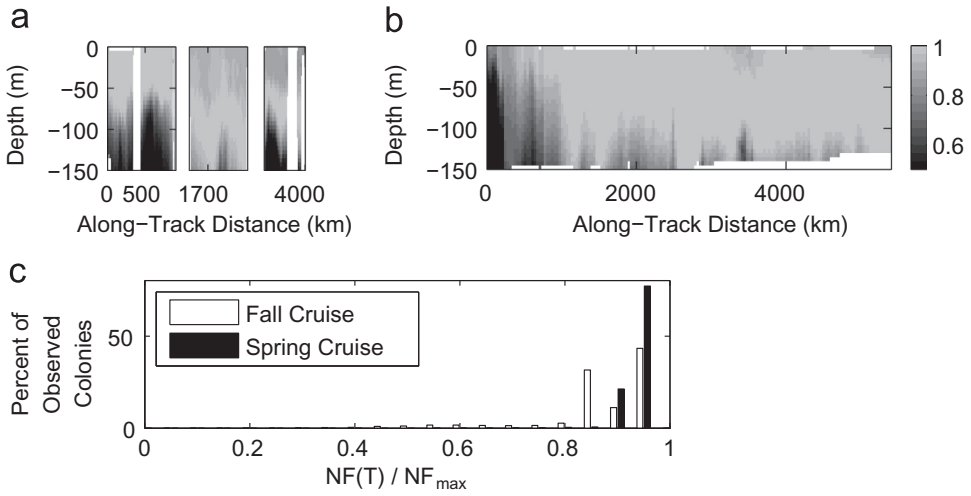

Fig. B1. Dependence of nitrogen fixation rate on temperature based on the empirical function $NF = -0.001096x^2 + 0.057x - 0.637$ (Breitbarth et al., 2007). Top panels display ratio of predicted to maximum N_2 fixation at temperatures observed during (a) fall 2010 and (b) the spring 2011. (c) Histogram of temperature dependence factor at temperatures experienced by individual colonies observed during the fall and spring cruises.

$$k = -\frac{d(\ln\ \phi)}{dz}. \tag{C.1}$$

Here, ϕ represents PAR. Because daytime PAR measurements were not available at all locations, we estimated single values for application to broad regions.

Attenuation coefficients were estimated from VPR PAR data binned to 5-m vertical resolution using Eq. (C.1) with the derivative estimated by central difference. They were reasonably homogeneous throughout the fall cruise but higher in regions of low salinity in spring (Fig. C1). Water associated with a freshwater lens observed on the spring cruise was turbid compared to the oceanic water observed elsewhere. Therefore, a single value for the fall cruise and dual values for the spring cruise (for salinities above and below 35.4) were chosen to minimize the least squares fit between the VPR-observed and estimated change in PAR over each bin.

The available PAR data were limited by a bias toward nighttime sampling and saturation of the PAR sensor at approximately 1200 μmol quanta m^{-2} s^{-1}. Quality control was achieved by eliminating bins with less than 545 or more than 2364 data points per bin and PAR values greater than 1150 μmol quanta m^{-2} s^{-1} or less than 10 μmol quanta m^{-2} s^{-1}, to minimize the effects of noise. The fitted attenuation coefficients at oceanic salinities were lower than the mean of the estimated attenuation coefficients over the corresponding regions, consistent with an observed tendency toward greater attenuation at depth, where PAR was less and therefore the effect on the mean square error was reduced. In the presence of uniform turbidity and parallel incident light, attenuation increases with depth due to the changing angular distribution and upward scattering of downwelling irradiance (Kirk, 1994, pp. 160–161).

Variability in attenuation coefficients with depth was similar in magnitude to variability among values at a single depth (Fig. C2). Therefore, only limited improvement in accuracy of the light field could be gained through specification of depth-varying attenuation coefficients. The difference in attenuation coefficient in the freshwater region of the spring cruise was much larger in

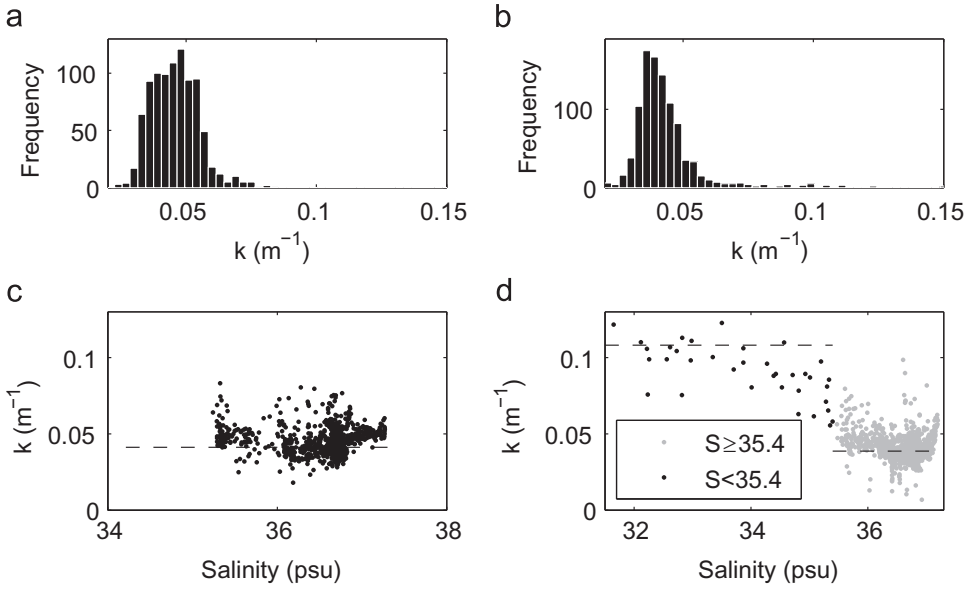

Fig. C1. Vertical attenuation coefficients estimated from VPR PAR measurements and Eq. (C.1). *Upper*: Histograms display distributions from (a) fall and (b) spring. *Lower*: Scatter plots of attenuation coefficient versus salinity for (c) fall and (d) spring with gray dots indicating low salinity locations. Estimated attenuation coefficients minimizing mean square error are shown with dashed lines.

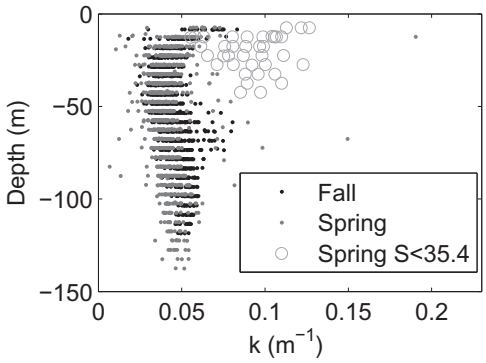

Fig. C2. Depth distribution of vertical attenuation coefficients estimated from VPR PAR measurements and Equation (C.1).

comparison.

Climatological PAR estimates were compared to PAR measured by the more recently calibrated PAR sensor used on CTD casts in order to validate the attenuation coefficients estimated based on the VPR PAR sensor (Fig. C3). The model and observations demonstrated broad agreement. Perfect agreement was not expected because of time-varying cloudiness in the observations.

Instantaneous PAR input to the nitrogen fixation model was estimated from daily PAR using

$$f(t) = I/I_d = \pi/24(A_1 + B_1\cos(W2))\frac{\cos(W2) - \cos(W1)}{\sin(W1) - W1\cos(W1)} \quad (C.2)$$

$$A_1 = 0.409 + 0.5016\sin(W1 - \pi/3) \quad (C.3)$$

$$B_1 = 0.6609 - 0.4767\sin(W1 - \pi/3) \quad (C.4)$$

where I is the instantaneous PAR and I_d is the daily PAR and all angles are in radians (Collares-Pereira and Rabl, 1979; Brock, 1981). $W1$, the sunset angle, and $W2$, the hour-angle, were calculated from Eqs. 3 and 5 found in Brock (1981, pp. 4–5).

Appendix D. Carbon per colony

Estimates of carbon content per colony were required to convert colony abundance to biomass estimates for input to the nitrogen fixation model (Fig. 2). Mean carbon contents per puff and raft colony were estimated by multiple linear regression of carbon content with number of puffs and number of rafts in each sample for each cruise (Table D1). This calculation was based on 101 samples for fall and 97 samples for spring. Bowtie carbon content per colony was assumed the same as puff content.

Table D1
Carbon per colony (μmol C colony^{-1}). Morphology-specific estimates were made by linear regression. Also shown are the standard error of the mean (where applicable) and estimated error variances ((μmol C colony^{-1})^2). The ranges are reported for each cruise. Very few samples fell near the upper range reported for OC469.

Group	Estimate	SEM	Variance	Range
OC469	0.64	0.36		0.1–5.1
OC469 puffs	0.31		0.0083	
OC469 rafts	0.67		0.0032	
OC471	0.82	0.11		0.2–1.9
OC471 puffs	0.62		0.0065	
OC471 rafts	0.94		0.0036	
Combined	0.73	0.003		
Combined puffs	0.55		0.0041	
Combined rafts	0.84		0.0020	

Variations in colony carbon content with depth were small compared to the ranges of values observed at single depths (not shown). Mean carbon per colony was higher for the spring cruise than for the fall cruise (Table D1); a Student's t-test demonstrated that the means were different at the 5% significance level ($p=0.01$). During both cruises, rafts had higher estimated carbon content than puffs. The tendency for greater raft carbon content compared to puff colonies was consistent with Orcutt et al. (2013) findings. There was little change in carbon per colony with latitude (Fig. D1).

Appendix E. Assessment of standard error in nitrogen fixation estimates

E.1. Calculation of standard error of the mean

In Table D1 and Figs. 9 and 10, a standard error of the mean is presented along with the estimate of mean nitrogen fixation or abundance. In calculating the standard error of the mean, we adjusted for autocorrelation within the sample as in Emery and Thomson (1997, p. 262). The standard error was calculated using the following equation:

$$SE = \frac{SD}{\sqrt{N_*}}, \quad (E.1)$$

where SD is the unbiased standard deviation

$$SD = \sqrt{\frac{1}{N-1}\sum_i^N (x_i - \bar{x})^2}, \quad (E.2)$$

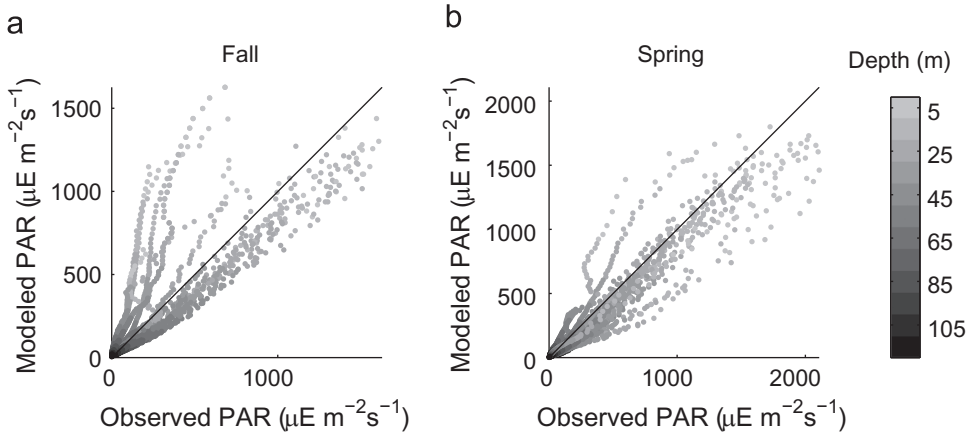

Fig. C3. Modeled vs. observed irradiance from (a) fall and (b) spring.

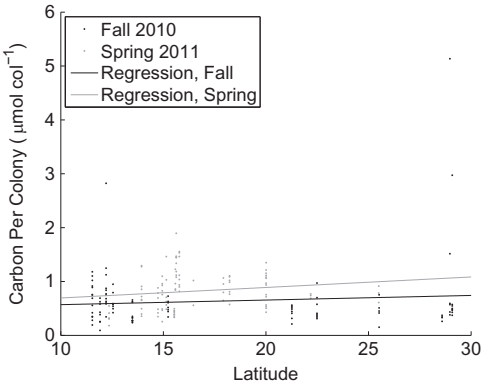

Fig. D1. Carbon content per colony versus latitude for all samples analyzed from the fall and spring cruises. Dotted lines show linear best fit to data.

and N^* is the effective sample size adjusted for spatial autocorrelation

$$N^* = \frac{N\Delta l}{\Lambda} \tag{E.3}$$

where N is the total number of samples and Δl is the sampling interval.

Λ is the integral length scale, the integral of the normalized autocorrelation function. The integral length scale is approximated by the summation of the normalized autocorrelation function up to the first zero crossing (Glover et al., 2011; Emery and Thomson, 1997):

$$\Lambda \approx \frac{\Delta l}{2C(0)} \sum_{k=0}^{n} (C(k) + C(k+1)) \tag{E.4}$$

where $C(k)$ is the autocovariance at lag k, and n is the index of the first zero crossing of the autocorrelation function. Integral length scales were estimated separately for nitrogen fixation and abundance in 5-m vertical depth bins covering each cruise.

E.2. Estimation of standard error associated with nitrogen fixation model

In order to quantify the uncertainty associated with predictions of nitrogen fixation, we estimated the expected variance. The variance of a function of several quantities, each with known variance, may be approximated using the delta method, derived using a Taylor expansion retaining second order terms (Mood et al., 1973, p. 181). Standard errors estimated by this methods are presented in Figs. 3 and 4.

We denote the individual input variables and parameters contributing to the variance in the function g as $X_1, X_2, \ldots, X_N$. The variance in g, $\mathrm{var}[g(X_1, X_2, \ldots, X_N)]$, is therefore the sum of the variance in each X_i times the square of the derivative of g with respect to X_i, plus twice the covariance of each pair (X_i, X_j) times the produce of the derivatives with respect to X_i and X_j:

$$\mathrm{var}[g(X_1, X_2, \ldots, X_N)] \approx \sum_{i}^{N} \sum_{j}^{N} \left(\frac{\partial g}{\partial X_i}\right)\left(\frac{\partial g}{\partial X_j}\right)\sigma_{ij} \tag{E.5}$$

where

$$\sigma_{ij} = \begin{cases} \mathrm{var}[X_i] & \text{if } i = j \\ \mathrm{cov}[X_i, X_j] & \text{if } i \neq j \end{cases} \tag{E.6}$$

σ_{ij} may be expressed as components of a symmetric variance–covariance matrix in which each of the diagonal elements represents a variance and each of the off-diagonal elements represents a covariance:

$$\sigma_{ij} = \begin{bmatrix} \sigma_{11} & \sigma_{12} & \cdots & \sigma_{1n} \\ \sigma_{21} & \sigma_{22} & \cdots & \sigma_{2n} \\ \vdots & \vdots & \ddots & \vdots \\ \sigma_{n1} & \sigma_{n2} & \cdots & \sigma_{nn} \end{bmatrix} \tag{E.7}$$

A summary of the application of the delta method to the model equations used in this study follows. The input quantities that are sources of variance in the estimate are the parameters α and μ; daily irradiance, I_d; attenuation coefficients, $k0$, $k1$, and $k2$; carbon per colony, *ccolR* and *ccolP*; and number of puffs+bowties and rafts, *PB* and *R*. Estimated parameter values and their associated variances and covariances are shown in Table E1. Variables *PB*, *R*, and I_d and their variances vary by location and therefore are not shown. In most cases, the covariance of different sources of variance are zero. However, in some instances, multiple parameters were estimated together from the same data, and the covariance between those parameters was considered.

E.2.1. Summary of model equations

Biomass:

$$B = (ccolR \times R + ccolP \times PB)C_{L:m3} \tag{E.8}$$

where *ccolR* is carbon per raft colony, *ccolP* is carbon per puff colony, *PB* is puff+bowtie colonies per L, *R* is raft colonies per L, $C_{L:m3} = 10^3\ \mathrm{L\ m^{-3}}$ is a conversion factor from $\mathrm{L^{-1}}$ to $\mathrm{m^{-3}}$.

Instantaneous irradiance:

Table E1
Estimated parameter values with associated variances. Also shown are parameter combinations with nonzero covariances. Units of variance are the square of the units of the estimated quantity. Units of covariance are the product of the units of the covarying quantities.

Parameter	Estimate	Variance	Covariance
α(μmol N(mol C)$^{-1}$ h^{-1}(μmol quanta m^{-2} s^{-1})$^{-1}$)	0.4175	2.310×10^{-3}	
μ (μmol N(mol C)$^{-1}$ h^{-1})	263.7	1524	
α, μ			−0.7738
$k0$ (m^{-1})	0.041	1.356×10^{-7}	
$k1$ (m^{-1})	0.039	2.762×10^{-7}	
$k2$ (m^{-1})	0.100	1.947×10^{-5}	
Fall *ccolR* (μmol C colony^{-1})	0.6693	3.173×10^{-15}	
Fall *ccolP* (μmol C colony^{-1})	0.3065	8.306×10^{-15}	
Fall *ccolR*, *ccolP*			-2.678×10^{-14}
Spring *ccolR* (μmol C colony^{-1})	0.9410	0.2553×10^{-15}	
Spring *ccolP* (μmol C colony^{-1})	0.6157	6.538×10^{-15}	
Spring *ccolR*, *ccolP*			-2.529×10^{-15}

$$I = \begin{cases} \dfrac{I_d f(t) \int_{-MLD}^{0} \exp\left(\int_0^z k(z)\, dz \right) dz}{MLD} & \text{if } z \geq -MLD \\ I_d f(t) \exp\left(\int_0^z k(z)\, dz \right) & \text{if } z < -MLD \end{cases} \tag{E.9}$$

where MLD is the depth of the mixed layer, I_d is the daily irradiance at the surface, $f(t)$ is a factor converting daily to instantaneous irradiance (Appendix C Eq. (C.2)), $k(z)$ is the attenuation coefficient. For the fall cruise, $k = 0.041\ \mathrm{m}^{-1}$ everywhere. For the spring cruise,

$$k = \begin{cases} 0.039 & \text{if } S \geq 35.4 \\ 0.100 & \text{if } S < 35.4 \end{cases} \tag{E.10}$$

Daily carbon-normalized nitrogen fixation:

$$F = \int_{day} \mu \tanh\left(\frac{\alpha I}{\mu} \right) dt \tag{E.11}$$

where α and μ are parameters associated with the nitrogen fixation model representing the initial slope and the asymptotic rate, respectively.

Total daily bulk nitrogen fixation:

$$NF = F \times B \tag{E.12}$$

E.2.2. Nitrogen fixation model parameters

The parameters α and μ were estimated by maximum likelihood (Section 3). We therefore estimate their variance and covariance from the Fisher information (Azzalini, 1996, pp. 68–84). The observed Fisher information matrix associated with a maximum likelihood estimate of parameters $(\theta_1, \theta_2, \ldots, \theta_n)$ is

$$\text{Fisher} = -\begin{bmatrix} \dfrac{\partial^2 LL}{\partial \theta_1^2} & \dfrac{\partial^2 LL}{\partial \theta_1 \partial \theta_2} & \cdots & \dfrac{\partial^2 LL}{\partial \theta_1 \partial \theta_n} \\ \dfrac{\partial^2 LL}{\partial \theta_2 \partial \theta_1} & \dfrac{\partial^2 LL}{\partial \theta_2^2} & \cdots & \dfrac{\partial^2 LL}{\partial \theta_2 \partial \theta_n} \\ \vdots & \vdots & \ddots & \vdots \\ \dfrac{\partial^2 LL}{\partial \theta_n \partial \theta_1} & \dfrac{\partial^2 LL}{\partial \theta_n \partial \theta_2} & \cdots & \dfrac{\partial^2 LL}{\partial \theta_n^2} \end{bmatrix} \tag{E.13}$$

where LL is the log likelihood and the derivatives are evaluated at the maximum likelihood estimates of all parameters. In the estimation of α and μ, we assume normally distributed random error (with variance ς^2) and the nitrogen fixation–irradiance relationship in Eq. (E.11). Then the log likelihood of the measured (I,F) pairs for given parameter values α, μ, and ς is

$$LL = -\frac{n}{2}\ln(2\pi) - n\ \ln\ \varsigma - \frac{\sum_i^n \left(\mu \tanh\left(\frac{\alpha I_i}{\mu} \right) - F_i \right)^2}{2\varsigma^2} \tag{E.14}$$

where (I_i, F_i) are paired incubation irradiances and nitrogen fixation measurements (2.1).

The variance–covariance matrix for the estimated parameters is approximately equal to the inverse of the Fisher information matrix:

$$\hat{\sigma} = \begin{bmatrix} \sigma_{11} & \sigma_{12} & \cdots & \sigma_{1n} \\ \sigma_{21} & \sigma_{22} & \cdots & \sigma_{2n} \\ \vdots & \vdots & \ddots & \vdots \\ \sigma_{n1} & \sigma_{n2} & \cdots & \sigma_{nn} \end{bmatrix} \approx \text{Fisher}^{-1} \tag{E.15}$$

The variance in NF due to variance in the nitrogen fixation model parameters α and μ is therefore approximately

$$\mathrm{var}(NF)_{\alpha,\mu} \approx \left(\frac{\partial NF}{\partial \alpha} \right)^2 \mathrm{var}(\alpha) + 2\frac{\partial NF}{\partial \alpha}\frac{\partial NF}{\partial \mu}\mathrm{cov}(\alpha, \mu) + \left(\frac{\partial NF}{\partial \mu} \right)^2 \mathrm{var}(\mu) \tag{E.16}$$

E.2.3. Daily surface irradiance

Variance associated with daily surface irradiance is estimated as the square of the standard deviations associated with the L3 SeaWiFS PAR product. The variance in NF due to I_d is therefore approximately

$$\mathrm{var}(NF)_{I_d} \approx \left(\frac{\partial NF}{\partial I_d} \right)^2 \mathrm{var}(I_d) \tag{E.17}$$

E.2.4. Attenuation coefficients

Each of the attenuation coefficients, k_0, k_1, and k_2, was estimated using a separate subset of data. k_0 was estimated using all available data points from the fall cruise meeting the quality control criteria described in Appendix C. All available quality-controlled data from the spring cruise from locations with salinity less than 35.4 were used to estimate k_2, while those with salinity greater than or equal to 35.4 were used to estimate k_1. Therefore, the estimated attenuation coefficients are independent, and their covariances zero. The least squares approach used to estimate each attenuation coefficient is equivalent to a maximum likelihood estimate under the assumption of normally distributed random error. The log likelihood is then

$$LL_k = -\frac{n}{2}\ln(2\pi) - n\ \ln\ \varsigma - \frac{\sum_i^n \left(I_{i,j-1/2} \exp(-kz_{i,j}) - I_{i,j+1/2} \right)^2}{2\varsigma^2} \tag{E.18}$$

where $I_{i,j}$ is the irradiance at the base of a given bin and $I_{i,j-1}$ is the irradiance at the top of the bin, k is the attenuation coefficient being estimated, either k_0, k_1, or k_2, and $z_{i,j}$ is the mean depth of the bin. The variances in k_0, k_1, and k_2 can then each be estimated by separate applications of Eqs. (E.13) and (E.15). The variances are then $\mathrm{var}(k_0) = \left(-\partial^2 LL_{k0}/\partial k_0^2 \right)^{-1}$, $\mathrm{var}(k_1) = \left(-\partial^2 LL_{k1}/\partial k_1^2 \right)^{-1}$, and $\mathrm{var}(k_2) = \left(-\partial^2 LL_{k2}/\partial k_2^2 \right)^{-1}$. The variance in NF due to the variance associated with the estimated attenuation coefficients is approximately

$$\mathrm{var}(NF)_k \approx \begin{cases} \left(\dfrac{\partial NF}{\partial k_0} \right)^2 \mathrm{var}(k_0) & \text{fall cruise} \\ \left(\dfrac{\partial NF}{\partial k_1} \right)^2 \mathrm{var}(k_1) + \left(\dfrac{\partial NF}{\partial k_2} \right)^2 \mathrm{var}(k_2) & \text{spring cruise} \end{cases} \tag{E.19}$$

E.2.5. Biomass parameters

Carbon per raft colony, *ccolR*, and carbon per puff colony, *ccolP*, were estimated by ordinary least squares. The problem consists of a design matrix $\mathbf{X}$ with columns of raft and puff colony numbers, a response vector $\mathbf{Y}$ of carbon contents, a vector $\mathbf{b}$ containing the parameters *ccolR* and *ccolP*, and a vector $\mathbf{e}$ of errors:

$$\mathbf{Y} = \mathbf{Xb} + \mathbf{e} \tag{E.20}$$

$\hat{\mathbf{b}}$ is the least squares estimate of $\mathbf{b}$:

$$\hat{\mathbf{b}} = \begin{bmatrix} ccolR \\ ccolP \end{bmatrix} \tag{E.21}$$

The estimated vector of residuals is

$$\hat{\mathbf{e}} = \mathbf{Y} - \mathbf{X}\hat{\mathbf{b}} \tag{E.22}$$

Thus the estimated variance–covariance matrix associated with the parameters *ccolR* and *ccolP* is

$$\begin{bmatrix} \mathrm{var}(ccolR) & \mathrm{cov}(ccolR, ccolP) \\ \mathrm{cov}(ccolR, ccolP) & \mathrm{var}(ccolP) \end{bmatrix} \approx \hat{\boldsymbol{\sigma}}_{\mathbf{ij}} = \frac{\hat{\mathbf{e}}^T\hat{\mathbf{e}}}{n-p}(\mathbf{X}^T\mathbf{X})^{-1} \tag{E.23}$$

The variance in *NF* due to variance in the parameters *ccolR* and *ccolP* is approximately

$$\begin{aligned} \mathrm{var}(NF)_{ccolR,ccolP} \approx & \left(\frac{\partial NF}{\partial ccolR}\right)^2 \mathrm{var}(ccolR) \\ & + 2\frac{\partial NF}{\partial ccolR}\frac{\partial NF}{\partial ccolP}\mathrm{cov}(ccolR, ccolP) \\ & + \left(\frac{\partial NF}{\partial ccolP}\right)^2 \mathrm{var}(ccolP) \end{aligned} \tag{E.24}$$

E.2.6. Colony abundance

Colony abundances and their variances were calculated under the assumption of a Poisson distribution. V_i is the volume sampled in each grid cell and n_i is the number of colonies in that cell. Then the abundance is given by

$$r_i = \frac{n_i}{V_i} \tag{E.25}$$

and the variance

$$\mathrm{var}(r_i) = \frac{r_i}{V_i}. \tag{E.26}$$

The variance in *NF* due to variance in raft abundance is estimated to be approximately

$$\mathrm{var}(NF)_R \approx \left(\frac{\partial NF}{\partial R}\right)^2 \mathrm{var}(R) \tag{E.27}$$

The variance in *NF* due to variance in puff and bowtie abundance is approximately

$$\mathrm{var}(NF)_{PB} \approx \left(\frac{\partial NF}{\partial R}\right)^2 \mathrm{var}(PB) \tag{E.28}$$

where *PB* is the combined abundance of puffs and rafts.

E.2.7. Total variance

The variance in bulk daily nitrogen fixation is estimated as the sum of each of the individual components:

$$\begin{aligned} \mathrm{var}(NF) \approx & \mathrm{var}(NF)_{\alpha,\mu} + \mathrm{var}(NF)_{I_d} + \mathrm{var}(NF)_k + \mathrm{var}(NF)_{ccolR,ccolP} \\ & + \mathrm{var}(NF)_R + \mathrm{var}(NF)_{PB} \end{aligned} \tag{E.29}$$

The standard error associated with the model is the square root of the model variance:

$$SE \approx \sqrt{\mathrm{var}(NF)} \tag{E.30}$$

E.3. Model variance in means of daily bulk nitrogen fixation estimates

In Fig. 10 we present means of modeled daily bulk nitrogen fixation estimates from multiple grid locations. We estimate the associated error in mean daily bulk nitrogen fixation by treating the calculation of the mean as part of the model:

$$M = \frac{1}{N}\sum_i^N NF_i \tag{E.31}$$

$$\mathrm{var}(M)_X = \left(\frac{\partial M}{\partial X}\right)^2 \mathrm{var}(X) \tag{E.32}$$

For the parameters, α, μ, k_0, k_1, and k_2, *ccolR*, and *ccolP*, single values with associated variances apply throughout each cruise. *ccolR* and *ccolP* vary by cruise and therefore must be treated separately for each cruise. For each of these parameters, the variance is calculated from the expression:

$$\mathrm{var}(M)_X = \left(\frac{\partial M}{\partial X}\right)^2 \mathrm{var}(X) = \frac{1}{N^2}\left(\sum_i^N \left(\frac{\partial NF}{\partial X}\right)_i\right)^2 \mathrm{var}(X) \tag{E.33}$$

The colony abundances, *R* and *PB*, and their variances vary by location with zero covariance, and therefore the value in each bin is considered individually as a separate source of variance. Since abundance in each bin is estimated individually, covariances of colony abundance estimates between bins are zero. The variance is therefore the sum of the variance associated with each individual bin:

$$\mathrm{var}(M)_X \approx \sum_i^N \left(\frac{\partial M}{\partial X_i}\right)^2 \mathrm{var}(X_i) = \frac{1}{N^2}\sum_i^N \left(\frac{\partial NF}{\partial X_i}\right)^2 \mathrm{var}(X_i) \tag{E.34}$$

The daily surface irradiance, I_d, and its variance vary laterally. Additionally, lateral covariances in I_d are unknown and assumed to be zero. Therefore in a lateral average, I_d is treated by applying Eq. (E.34).

Appendix F. Nitrogen fixation method comparison

A comparison was made between nitrogen fixation measurements made by $^{15}N_2$ incubation and acetylene reduction assay over subset of data used in the present study (Fig. F1). The results were consistent with the global comparison made by Luo et al. (2012) and did not reveal a systematic bias.

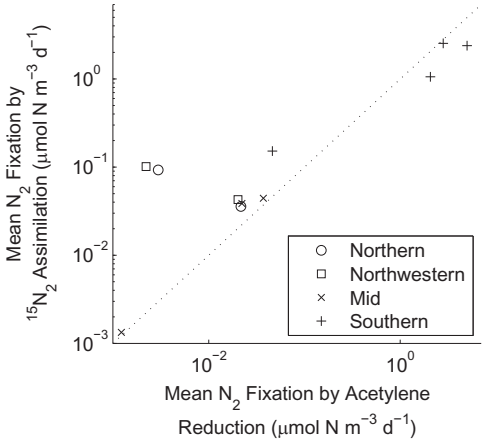

Fig. F1. Comparison of mean N_2 fixation: $^{15}N_2$ assimilation vs. acetylene reduction assay. Values presented are means of data included in the Luo et al. (2012) database for each of the depths and the four geographical regions displayed in Fig. 10.

References

Andresen, E., Lohscheider, J., Šetlikova, E., Adamska, I., Šimek, M., Küpper, H., 2010. Acclimation of *Trichodesmium erythraeum* ISM101 to high and low irradiance analysed on the physiological, biophysical and biochemical level. New Phytol. 185, 173–188.

Azzalini, A., 1996. Statistical Inference Based on the Likelihood. Chapman & Hall/CRC, London.

Berman-Frank, I., Quigg, A., Finkel, Z.V., Irwin, A.J., Haramaty, L., 2007. Nitrogen-fixation strategies and Fe requirements in cyanobacteria. Limnol. Oceanogr. 52, 2260–2269.

Breitbarth, E., Oschlies, A., LaRoche, J., 2007. Physiological constraints on the global distribution of *Trichodesmium*—effect of temperature on diazotrophy. Biogeosciences 4, 53–61.

Breitbarth, E., Wohlers, J., Kläs, J., LaRoche, J., Peeken, I., 2008. Nitrogen fixation and growth rates of *Trichodesmium* IMS-101 as a function of light intensity. Mar. Ecol. Prog. Ser. 359, 25–36.

Brock, T.D., 1981. Calculating solar radiation for ecological studies. Ecol. Model. 14, 1–19.

Capone, D.G., Burns, J.A., Montoya, J.P., Subramaniam, A., Mahaffey, C., Gunderson, T., Michaels, A.F., Carpenter, E.J., 2005. Nitrogen fixation by *Trichodesmium* spp.: an important source of new nitrogen to the tropical and subtropical North Atlantic Ocean. Glob. Biogeochem. Cycles 19, GB2024. http://dx.doi.org/10.1029/2004GB002331.

Capone, D.G., Montoya, J.P., 2001. Nitrogen fixation and denitrification.. In: Paul, J.H. (Ed.), Marine Microbiology, Methods in Microbiology vol. 30. Academic Press, St Petersburg, Florida, pp. 501–515. http://dx.doi.org/10.1016/S0580-9517(01)30060-0.

Carpenter, E.J., Subramaniam, A., Capone, D.G., 2004. Biomass and primary productivity of the cyanobacterium *Trichodesmium* spp. in the tropical N Atlantic ocean. Deep-Sea Res. I 51, 173–203.

Chappell, P.D., Webb, E.A., 2010. A molecular assessment of the iron stress response in the two phylogenetic clades of *Trichodesmium*. Environ. Microbiol. 12 (1), 13–27.

Chen, Y.-B., Zehr, J.P., Mellon, M., 1996. Growth and nitrogen fixation of the diazotrophic filamentous nonheterocystous cyanobacterium *Trichodesmium* sp. IMS 101 in defined media: evidence for a circadian rhythm. J. Phycol. 32, 916–923.

Codispoti, L.A., Brandes, J.A., Christensen, J.P., Devol, A.H., Naqvi, S.W.A., Paerl, H.W., Yoshinari, T., 2001. The oceanic fixed nitrogen and nitrous oxide budgets: moving targets as we enter the anthropocene?. Sci. Marina 65 (Suppl. 2), 85–105.

Coles, V.J., Wilson, C., Hood, R.R., 2004. Remote sensing of new production fueled by nitrogen fixation. Geophys. Res. Lett. 31, L06301. http://dx.doi.org/10.1029/2003GL019018.

Collares-Pereira, M., Rabl, A., 1979. The average distribution of solar-radiation correlations between diffuse and hemispherical, and between daily and hourly instolation values. Sol. Energy 22, 155–168.

Davis, C.S., McGillicuddy, D.J., 2006. Transatlantic abundance of the N_2-fixing colonial cyanobacterium *Trichodesmium*. Science 312 (5779), 1517–1520. http://dx.doi.org/10.1126/science.1123570.

Davis, C.S., Thwaites, F.T., Gallager, S.M., Hu, Q., 2005. A three-axis fast-tow digital video plankton recorder for rapid surveys of plankton taxa and hydrography. Limnol. Oceanogr. Methods 3, 59–74.

Deutsch, C., Sarmiento, J.L., Sigman, D.M., Gruber, N., Dunne, J.P., 2007. Spatial coupling of nitrogen inputs and losses in the ocean. Nature 445, 163–167.

Emery, W.J., Thomson, R.E., 1997. Data Analysis Methods in Physical Oceanography. Pergamon, Oxford, UK.

Fu, F.-X., Bell, P.R.F., 2003. Factors affecting N_2 fixation by the cyanobacterium *Trichodesmium* sp. GBRTRLI101. FEMS Microbiol. Ecol. 45, 203–209. http://dx.doi.org/10.1016/S0168-6496(03)00157-0.

Galloway, J.N., et al., 2004. Nitrogen cycles: past, present, and future. Biogeochemistry 70, 153–226.

Glover, D.M., Jenkins, W.J., Doney, S.C., 2011. Modeling Methods for Marine Science. Cambridge University Press.

Gruber, N., 2004. The dynamics of the marine nitrogen cycle and its influence on atmospheric CO_2. In: Follows, M., Oguz, T. (Eds.), The Ocean Carbon Cycle and Climate, NATO ASI Series. Kluwer Academic, Dordrecht, pp. 97–148.

Gruber, N., 2008. The marine nitrogen cycle: overview and challenges. In: Capone, D.G., Bronk, D.A., Mulholland, M.R., Carpenter, E.J. (Eds.), Nitrogen in the Marine Environment. Elsevier, Amsterdam, The Netherlands, pp. 1–50.

Heithoff, A., 2011. N_2 Fixation by Subsurface Populations of *Trichodesmium*: an Important Source of new Nitrogen to the North Atlantic Ocean (MS Thesis). Department of Biology, Massachusetts Institute of Technology and the Woods Hole Oceanographic Institution.

Hood, R.R., Subramaniam, A., May, L.R., Carpenter, E.J., Capone, D.G., 2002. Remote estimation of nitrogen fixation by *Trichodesmium*. Deep-Sea Res. II 49, 123–147.

Hu, Q., Davis, C., 2006. Accurate automatic quantification of taxa-specific plankton abundance using dual classification with correction. Mar. Ecol. Prog. Ser. 306, 51–61.

Hutchins, D.A., Fu, F.-X., Zhang, Y., Warner, M.E., Feng, Y., Portune, K., Bernhardt, P.W., Mulholland, M.R., 2007. CO_2 control of *Trichodesmium* N_2 fixation, photosynthesis, growth rates, and elemental ratios: implications for past present and future ocean biogeochemistry. Limnol. Oceanogr. 52 (4), 1293–1304.

Hynes, A.M., Webb, E.A., Doney, S.C., Waterbury, J.B., 2012. Comparison of cultured *Trichodesmium* (Cyanophyceae) with species characterized from the field. J. Phycol. 48, 196–210. http://dx.doi.org/10.1111/j.1529-8817.2011.01096.x.

Jenkins, W., Goldman, J., 1985. Seasonal oxygen cycling and primary production in the Sargasso Sea. J. Mar. Res. 43 (2), 465–491.

Kirk, J.T.O., 1994. Light and Photosynthesis in Aquatic Ecosystems. Cambridge University Press, Cambridge, England.

Letelier, R.M., Karl, D.M., 1998. *Trichodesmium* spp. physiology and nutrient fluxes in the North Pacific subtropical gyre. Aquat. Microb. Ecol. 15, 265–276.

Levitan, O., Brown, C.M., Sudhaus, S., Campbell, D., LaRoche, J., Berman-Frank, I., 2010. Regulation of nitrogen metabolism in the marine diazotroph *Trichodesmium* IMS101 under varying temperatures and atmospheric CO_2 concentrations. Environ. Microbiol. 12 (7), 1899–1912. http://dx.doi.org/10.1111/j.1462-2920.2010.02195.x.

Luo, Y.-W., et al., 2012. Database of diazotrophs in global ocean: abundance, biomass and nitrogen fixation rates. Earth Syst. Sci. Data 4, 47–73.

Mills, M.M., Ridame, C., Davey, M., La Roche, J., 2004. Iron and phosphorus co-limit nitrogen fixation in the eastern tropical North Atlantic. Nature 429, 292–294.

Mohr, W., Großkopf, T., Wallace, D.W.R., LaRoche, J., 2010. Methodological underestimation of oceanic nitrogen fixation rates. PLoS ONE 5 (9), e12583. http://dx.doi.org/10.1371/journal.pone.0012583.

Mood, A.M., Graybill, F.A., Boes, D.C., 1973. Introduction to The theory of Statistics. McGraw-Hill, New York.

Mulholland, M.R., Bernhardt, P.W., Heil, C.A., Bronk, D.A., O'Neil, J.M., 2006. Nitrogen fixation and release of fixed nitrogen by *Trichodesmium* spp. in the Gulf of Mexico. Limnol. Oceanogr. 51, 1762–1776.

Ohki, K., Zehr, J.P., Fujita, Y., 1992. Regulation of nitrogenase activity in relation to the light-dark regime in the filamentous non-heterocystous cyanobacterium *Trichodesmium* sp. NIBB 1067. J. Gen. Microbiol. 138, 2679–2685.

Olson, E.M., 2014. Investigating the Role of *Trichodesmium* spp. in the Oceanic Nitrogen Cycle through Observations and Models (Ph.D. thesis). Massachusetts Institute of Technology and the Woods Hole Oceanographic Institution.

Orchard, E.D., Webb, E.A., Dyhrman, S.T., 2009. Molecular analysis of the phosphorus starvation response in *Trichodesmium* spp. Environ. Microbiol. 11 (9), 2400–2411. http://dx.doi.org/10.1111/j.1462-2920.2009.01968.x.

Orcutt, K.M., Lipschultz, F., Gundersen, K., Arimoto, R., Michaels, A.F., Knap, A.H., Gallon, J.R., 2001. A seasonal study of the significance of N_2 fixation by *Trichodesmium* spp. at the Bermuda Atlantic Time-series Study (BATS) site. Deep-Sea Res. II 48, 1583–1608.

Orcutt, K.M., Gundersen, K., Ammerman, J.W., 2013. Intense ectoenzyme activities associated with *Trichodesmium* colonies in the Sargasso Sea. Mar. Ecol. Prog. Ser. 478, 101–113. http://dx.doi.org/10.3354/meps10153.

Orcutt, K.M., Rasmussen, U., Webb, E.A., Waterbury, J.B., Gundersen, K., Bergman, B., 2002. Characterization of *Trichodesmium* spp. by genetic techniques. Appl. Environ. Microbiol. 68 (5), 2236–2245. http://dx.doi.org/10.1128/AEM.68.5.22362245.2002.

Platt, T., Harrison, W.G., 1985. Biogenic fluxes of carbon and oxygen in the ocean. Nature 318, 55–58.

Post, A.F., et al., 2002. Spatial and temporal distribution of *Trichodesmium* spp. in the stratified Gulf of Aqaba, Red Sea. Mar. Ecol. Prog. Ser. 239, 241–250.

Rabouille, S., Staal, M., Stal, L.J., Soetaert, K., 2006. Modeling the dynamic regulation of nitrogen fixation in the cyanobacterium *Trichodesmium* sp. Appl. Environ. Microbiol. 72 (5), 3217–3227. http://dx.doi.org/10.1128/AEM.72.5.32173227.2006.

Rodier, M., Borgne, R.L., 2010. Population and trophic dynamics of *Trichodesmium thiebautii* in the SE lagoon of New Caledonia Comparison with *T. erythraeum* in the SW lagoon. Mar. Pollut. Bull. 61, 349–359.

Rouco, M., Joy-Warren, H., McGillicuddy, D.J., Waterbury, J.B., Dyhrman, S.T., 2014. *Trichodesmium* sp. clade distributions in the western North Atlantic Ocean. Limnol. Oceanogr. 59 (6), 1899–1909. http://dx.doi.org/10.4319/lo.2014.59.6.1899.

Saino, T., Hattori, A., 1978. Diel variation in nitrogen fixation by a marine blue-green alga *Trichodesmium thiebautii*. Deep-Sea Res. 25, 1259–1263.

Sañudo-Wilhelmy, S.A., et al., 2001. Phosphorus limitation of nitrogen fixation by *Trichodesmium* in the central Atlantic Ocean. Nature 441, 66–69.

Shulenberger, E., Reid, J.L., 1981. The pacific shallow oxygen maximum, deep chlorophyll maximum, and primary productivity, reconsidered. Deep-Sea Res. 28A (9), 901–919.

Subramaniam, A., et al., 2008. Amazon River enhances diazotrophy and carbon sequestration in the tropical North Atlantic Ocean. Proc.Natl. Acad. Sci. 105 (30), 10,460–10,465.

Tovar-Sanchez, A., Sañudo-Wilhelmy, S.A., 2011. Influence of the Amazon River on dissolved and intra-cellular metal concentrations in *Trichodesmium* colonies along the western boundary of the sub-tropical North Atlantic Ocean. Biogeosciences 8, 217–225. http://dx.doi.org/10.5194/bg-8-217-2011.

Villareal, T.A., Carpenter, E.J., 2003. Buoyancy regulation and the potential for vertical migration in the oceanic cyanobacterium *Trichodesmium*. Microb. Ecol. 45 (1), 1–10.

Walsby, A.E., 1978. The properties and buoyancy-providing role of gas vacuoles in *Trichodesmium ehrenberg*. Br. Phycol. J. 13, 103–116.

Westberry, T., Siegel, D., Subramaniam, A., 2005. An improved bio-optical model for

the remote sensing of *Trichodesmium* spp. blooms. J. Geophys. Res.–Oceans 110 (C6) http://dx.doi.org/10.1029/2004JC002517.
Westberry, T.K., Siegel, D.A., 2006. Spatial and temporal distribution of *Trichodesmium* blooms in the world's oceans. Glob. Biogeochem. Cycles 20 (4) http://dx.doi.org/10.1029/2005GB002673.
White, A.E., Spitz, Y.H., Letelier, R.M., 2006. Modeling carbohydrate ballasting by *Trichodesmium* spp. Mar. Ecol. Prog. Ser. 323, 35–45.
Wilson, S.T., Böttjer, D., Church, M.J., Karl, D.M., 2012a. Comparative assessment of nitrogen fixation methodologies, conducted in the oligotrophic North Pacific Ocean. Appl. Environ. Microbiol. 78 (18), 6516–6523. http://dx.doi.org/10.1128/AEM.01146-12.
Wilson, S.T., Kolber, Z.S., Tazzi, S., Zehr, J.P., Karl, D.M., 2012b. Nitrogen fixation hydrogen cycling and electron transport kinetics in *Trichodesmium erythraeum* (cyanobacteria) strain IMS101. J. Phycol. 48, 595–606.